Masterthesis

Nonmodal stability analysis of the interface between aqueous humor and vitreous substitutes after vitreoretinal surgery

by
Aulikki Wilhelmi genannt Hofmann *

submitted to the
Department of Mathematics
at **Universität Hamburg**

performed at the
DICCA
Department of Civil, Chemical and Environmental Engineering

Università degli Studi di Genova, Italia

under the guidance of Ric. Jan Oskar Pralits†

Supervisor: Prof. Rodolfo Repetto
Second examiner: Prof. Dr. Ingenuin Gasser

14. 07. 2017

*matriculation number: 6584881; mailto: aulikki.wilhelmi@studium.uni-hamburg.de
†mailto: jan.pralits@unige.it

Abstract

In case of retinal detachment in the human eye, blindness can be prevented by vitrectomy, a surgical procedure in which the vitreous body gets replaced by a tamponade fluid. In most cases emulsification occurs after some time which can lead to serious sight problems. A simple model of the flow in a vitrectomized eye is a flow of two superposed fluids over an oscillating flat plate. In order to understand emulsification processes better also short-term influences should be examined. The results of a nonmodal stability analysis on a two-fluid Stokes flow has not been published jet. This investigation is new to the field of fluid mechanics.

As the mathematical model ended up in a constraint optimization problem, for the implementation the question arose how the discretization should be done. The approach *first optimized, then discretized* was applied as the contrary approach led to numerical problems at the interface. For that the continuous adjoint equations, interface and boundary conditions were necessary. The verification of the code used for the numerical experiments was done by comparison with a nonmodal analysis of a classical single-fluid Stokes flow.

A parameter study with values relevant to the problem was done. The perturbations which led to maximal transient growth were waves with a zero spanwise wavenumber. The influence of the initial and final instant of time on the optimal parameters was crucial and could be led back to the shape of the base flow at that time. The damping influence of the viscosity-ratio m of the fluids appeared with $m > 1$ and grew with it. The question if and to what extent nonmodal transient growth influences the stability of the interface between aqueous humor and a tamponade fluid, followed from the application. The results of this work show that in a situation which is realistic for the eye, the flow is fully damped and no critical energy rising appears. Thus, unstable behavior which might lead to emulsification in the eye due to short-term transient growth rise can be excluded.

Ehrenwörtliche Versicherung

Die vorliegende Arbeit habe ich selbständig verfasst und keine anderen als die angegebenen Hilfsmittel - insbesondere keine im Quellenverzeichnis nicht benannten Internet-Quellen - benutzt. Die Arbeit habe ich vorher nicht in einem anderen Prüfungsverfahren eingereicht. Die eingereichte schriftliche Fassung entspricht genau der auf dem elektronischen Speichermedium.

Declaration of Authorship

I have written the present thesis by my own and have not used other than the acknowledged resources and aids - especially no uncited internet sources. I have not handed in this thesis in another examination procedure. The submitted written version corresponds to the version on the electronic storage medium.

Hamburg, den 14. 07. 2017

Acknowledgements

I would like to express my sincere gratitude to **Jan O. Pralits** from the department of Civil, Chemical and Environmental Engineering at the University Genova for his warm welcome when I arrived in Genova and his guidance throughout this work. I am thankful for his patience, time and knowledge he shared with me always focused on my learning success. I am grateful for his very valuable comments and advises.

Moreover I express my deepest thanks to my supervisor **Rodolfo Repetto** from the department of Civil, Chemical and Environmental Engineering at the University Genova and my second examiner **Ingenuin Gasser** from the Department of Mathematics at the University of Hamburg for their supervision as it gave me the possibility of this transnational work.

Contents

List of Figures

List of Tables

Nomenclature

Mathematical Symbols

Symbol	Meaning
$\epsilon \ll 1$	arbitrarily small positive quantity
$\mathcal{O}(\ )$	of order
$\boldsymbol{u}$	bold small letters: column vector
$\frac{\partial}{\partial x}$	partial derivative w.r.t. x
$\boldsymbol{\nabla} = (\frac{\partial}{\partial x}, \frac{\partial}{\partial y}, \frac{\partial}{\partial z})^T$	nabla operator
$\boldsymbol{\Delta u}$	Laplace operator
$\boldsymbol{M}$	bold capital letters: matrix (exception: base flow)
$\mathbb{C}$	set of complex numbers
$\mathbb{C}^{n\times n}$	space of complex matrices with dimension $n \times n$
$\mathbb{C}^n$	space of complex vectors with dimension n
$\| \|$	a norm
$\|_{-1}$	inversion of a matrix
$\mathcal{K}(\ )$	condition number of a matrix
$G(t)$	gain function
$\| \|_{spec}$	spectral-norm
$i = \sqrt{-1}$	imaginary unit
$\| \|$	modulus
$D\ ,\ '$	first partial derivative w.r.t. y
$D^2\ ,\ ''$	second partial derivative w.r.t. y
$\| \|_E$	energy-norm
$\|_H$	conjugate transposed
$\| \|_{L_2}$	L_2-norm
$\|_T$	transposed
$div(\ )$	divergence of a vector
$(\ ,\ )$	inner product w.r.t. the euclidean norm
$\times$	cross product between two vectors $\in \mathbb{R}^3$
$\mathfrak{R}(\ )$	real part of an argument
c_c	complex conjugate
$\nabla = \frac{\partial}{\partial x} + \frac{\partial}{\partial y} + \frac{\partial}{\partial z}$	-
$\nabla^2 = \frac{\partial^2}{\partial x^2} + \frac{\partial^2}{\partial y^2} + \frac{\partial^2}{\partial z^2}$	-
$\boldsymbol{\Delta} = (\nabla^2, \nabla^2, \nabla^2)^T$	-
$(\ ,\ )_{\boldsymbol{M}}$	inner product w.r.t. matrix $\boldsymbol{M}$ s.p.d.

$\frac{D}{Dt}$	material derivative w.r.t. t
$\boldsymbol{n}$	outer normal vector on the interface
$\boldsymbol{t}$	tangential vector on the interface
H	mean curvature of the interface
$\nabla_{\parallel} = \boldsymbol{\nabla} - \boldsymbol{n}(\boldsymbol{n}, \boldsymbol{\nabla})$	surface gradient
$\boldsymbol{T}_j^{\xi}$	stress tensors at the interface
$J(T)$	cost functional depending on final time T
$s.t.$	subject to
$_d$	spacially discretized quantity
$\mathcal{L}$	Lagrange functional
$_a$	adjoint variable

Physical Symbols

Symbol	Unit	Meaning
$\hat{}$	-	perturbed quantities
α	-	streamwise wavenumber
β	-	spanwise wavenumber
$k = \sqrt{\alpha^2 + \beta^2}$	-	-
T	-	dimensionless final instant in time
*		dimensionful variables
$\rho^* = \frac{\mu^*}{\nu^*}$	$\frac{kg\,m}{s^2}$	density
ν^*	$\frac{m^2}{s}$	kinematic viscosity
μ^*	$\frac{kg}{m\,s}$	dynamic viscosity
δ^*	m	thickness of outer fluid (fluid 1)
$\boldsymbol{x}^* = (x^*, y^*, z^*)^T$	$\frac{m}{s}$	spatial vector with components
ω^*	$\frac{1}{s}$	frequency of moving plate
u_0^*	$\frac{m}{s}$	characteristic flow velocity
u_ω^*	$\frac{m}{s}$	velocity ot the wall
g^*	$\frac{m}{s^2}$	gravitational acceleration
$\boldsymbol{u}^* = (u^*, v^*, w^*)^T$	$\frac{m}{s}$	velocity vector with components
t^*	s	time
p^*	$\frac{kg}{m^2}$	pressure
$Re = \frac{u_0^* \delta^* \rho^*}{\mu *}$	-	dimensionless Reynolds number
$Fr = \sqrt{\frac{u_0^* \omega^*}{g^*}}$	-	dimensionless Froude number
$\gamma = \frac{\rho_2^*}{\rho_1^*}$	-	ratio of the densities
ξ	-	quantities exactly at interface
$m = \frac{\mu_2^*}{\mu_1^*}$	-	ratio of the dynamic viscosities
$\boldsymbol{U_j}$, U_j	-	base flow; bold capital letters: vector; capital letters: component of vector

Symbol	**Unit**	**Meaning**
ξ^*	m	deviation of the interface
η	-	normal vorticity
σ^*	$\frac{N}{m}$	surface tension
$E(t)$	-	energy depending on time t
Ω	-	whole domain
Ω_1	-	domain of fluid next to the wall
Ω_2	-	domain of fluid extending to infinity
E_q	-	flow energy
E_ξ	-	interface energy
$_B$	-	ω-independent scaling
$P^* = \frac{2\pi}{\omega^*}$	$\frac{1}{s}$	period
ν	-	spanwise vorticity
t_{in}	-	initial instant in time as ratio of a full period P
t_{fin}	-	final instant in time as ratio of a full period P

Chapter 1

Introduction

Even though Stevie Wonder supposedly once said that *"just because one lacks the use of its eyes doesn't mean one lacks vision"*, becoming blind is a frightening situation. This thesis might contribute to a better understanding of the reasons behind sight problems, in the worst case a complete loss of sight, due to emulsification after vitrectomy. Admittedly, this start seems to be dramatic but as science became so specialized every little step is a step forward and as Wonder taught us, the vision is important. But what is vitrectomy and how is emulsification involved?
Vitrectomy is a surgical treatment for retinal detachment (RD), which is a potential blinding condition of the eye (see Figure 1.1 on the left). Hereby, as it can be seen in the mentioned figure on the right, the retina detaches from the ciliary body due to which retina holes may occur. Those might even get worse due to eye motion and the detachment of the vitreous body.

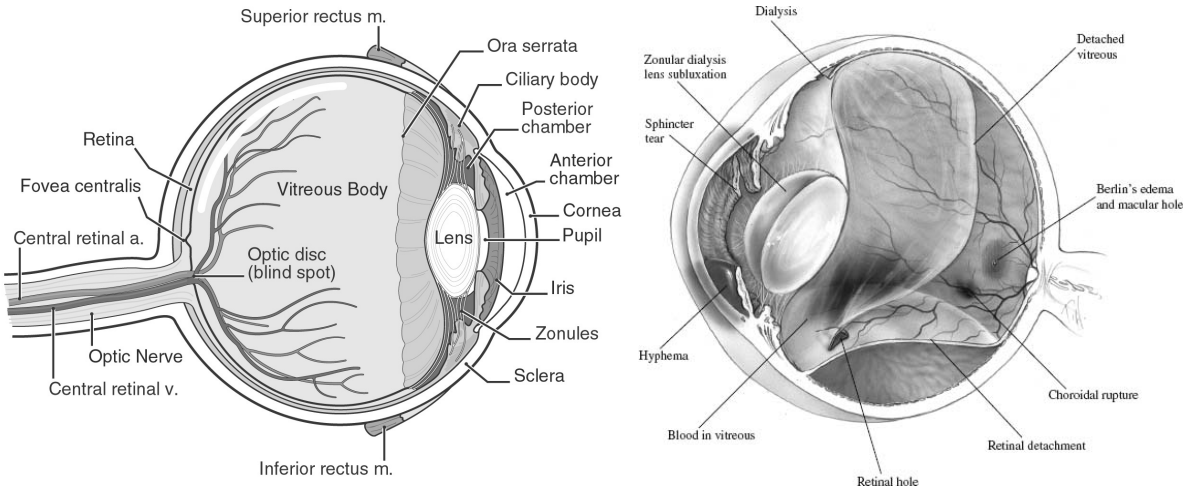

Fig. 1.1: Anatomy of the human eye (left) * ;Retinal detachment and related eye injuries (right) †

During the surgical procedure the vitreous body, which has a gelatinous texture, is cut in small pieces, removed from the vitreous chamber and replaced by a substitute. For this, various tamponade fluids can be used such as silicon oils, perfluorocarbon liquids

*08/07/2017: `http://humananatomychart.us/simple-human-body-diagram`
†08/07/2017: `https://entokey.com/vitreous-and-retina`

or gas, where the ideal one mimics the positive characteristics like elasticity and buffer capacity and avoids negative like biodegradability with age (Kleinberg et al., 2011, p. 300). The most often used silicon oils are immiscible with water which leads to a situation where two fluids are evident in the eye. As it is not possible to remove the aqueous humor completely from the vitreous chamber, some of it stays inside covering the retina. The filled-in tamponade fluid is forming a single drop in the place, once occupied by the vitreous body. It is most likely, due to the hydrophobic properties, that this drop does not come in contact with the retina. However, the aqueous humor might not be equally spread over the whole retina surface since the density difference will force most of it to the top or bottom (Isakova et al., 2014, p. 2). There will be areas where a very thin layer, others where a rather thick layer, of aqueous humor separates the retina from the vitreous substitute.
It has been observed that after some time these liquids tend to emulsify, which can lead to post-operative complications like cataract or glaucoma (Heimann et al., 2008, p. 3-5). Because of that risk the vitreous substitute has to be removed resulting in another surgical procedure for the patient. In order to find liquids which do not exhibits these emulsion effects, a better understanding of the aqueous-tamponade fluid interface is essential.

Emulsification of two immiscible fluids describes the appearing of drops separated from one fluid and entering the other fluid. In this particular case the interface between aqueous humor and tamponade fluid breaks down. It is presumed, that if this breakdown is happening near the wall, where the layer of aqueous humor is very thin, one can find a relation to the shear stresses at the interface induced by eye rotation (Isakova et al., 2014, p. 2). A simple model of this setting can be described by an oscillating flat plate with a thin domain of one fluid superposed by a second one on top. This thesis focuses on that model, as in areas further away from the wall other hydrodynamical effects like sloshing might dominate. In the mentioned paper of Isakova et al. (2014) a linear modal stability analysis has been done using a quasi steady approach where the basic flow is frozen for each instant in time and the eigenmodes of the perturbations are evaluated. The results obtained suggest that indeed shear stresses can promote the surface instability at least in terms of a long time behavior. But what happens after a short time? As Schmid (2007) stated in the introduction of his report, the spectrum of most wall-bounded shear flows gives an unsatisfying estimate for the perturbation behavior as it only describes the evolution for time $t \to \infty$. In order to get a more complete picture of interface-stability and thus a better understanding of emulsification, the objective of this work is a nonmodal stability analysis of the simple model mentioned above.

The governing equations of two superposed fluids over a moving plate have been subject to many publications, see e.g. Joseph and Renardy (1993). A nonmodal stability analysis has been done by Biau (2016) for an oscillatory Stokes flow and by Orazzo et al. (2014) for a core-annular flow. Few works exist regarding nonmodal stability analysis of interface flows. However, for single fluid shear flows the literature is quite broad.

An introduction on nonmodal stability analysis will be given in chapter 2. In chapter 3 a very detailed description on the mathematical formulation of the problem follows, ending

with the flow governing equations. chapter 4 concludes the theoretical part of this thesis by applying concepts from optimization to the formulated problem. The numerical verification of the code in comparison with the work of Biau (2016) is presented in chapter 5. The results of the numerical experiments for the two-fluid case are content of chapter 6. A conclusion and some recommendations for further work in chapter 7 mark the end of this thesis.

Chapter 2

Nonmodal Stability-analysis

This chapter is mostly based on the lecture given by J. Pralits at the University of Genova (Italy) in Feburary 2017 which he mainly based on Schmid (2007). It focuses on the understanding of this method and its relevance for the problem considered here rather than being exhaustive. For this reason, after a short introduction, a small model problem will be presented and followed by a more realistic case concerning the flow this work investigates.

Stability analysis in fluid dynamics, seen as the behavior of a flow due to small perturbations, has long been dominated by the analysis solely of the eigenvalues of the governing linear operator where the least stable mode determines whether the flow is stable or unstable depending on its position in the complex plane. But the focus on the long-term behavior does not capture possible instabilities that might occur within a finite-time horizon, which might be of great interest in practical application. As an example, experiments in a plane Poiseuille flow showed that instabilities and transition already appear after a substantially shorter time than predicted from the least stable eigenmode (Schmid, 2007, p. 131) and at a subcritical Reynolds number i.e. at a value of the Reynolds number for which the flow is linearly stable. A measure for stability can be the kinetic energy and a flow is said to be stable if the energy goes to zero for $t \to \infty$. Stability can also be thought of as the response of a system to initial conditions or external forcing. It will be focused on the first approach giving rise to the question which initial conditions result in the largest amplification of the system. In fact this ends up in an optimization problem where a measure of the system is maximized under the constrained of fulfilling the governing flow equations. The choice of a measure becomes more complex if there is for example an interface involved. The following section makes some of these briefly outlined thoughts more evident.

2.1 A Model Problem

In order to arrive at the equations describing the behavior of perturbations $\hat{\boldsymbol{q}}(\boldsymbol{x}, t)$ we linearize the flow around a steady base flow $\boldsymbol{q_b}(\boldsymbol{x})$

$$\boldsymbol{q_b}(\boldsymbol{x}) + \epsilon\, \hat{\boldsymbol{q}}(\boldsymbol{x}, t) + \mathcal{O}(\epsilon^2) \tag{2.1}$$

with $\epsilon \ll 1$. $\hat{}$ will denote perturbed quantities throughout this work and bold letters indicate vectorial quantities. Inserting (2.1) in the Navier-Stokes equations, selecting

only the terms of order ϵ and neglecting all higher order terms, it follows

$$\frac{\partial \hat{\boldsymbol{q}}}{\partial t} = -(\hat{\boldsymbol{q}}, \boldsymbol{\nabla})\boldsymbol{q_b} - (\boldsymbol{q_b}, \boldsymbol{\nabla})\hat{\boldsymbol{q}} - \boldsymbol{\nabla}\hat{p} + \frac{1}{Re}\Delta\hat{\boldsymbol{q}}, \tag{2.2}$$

having in mind that the Navier-Stokes equations are also valid for the base flow. For further explanations about the symbols and equations in particular see the Nomenclature and subsection 3.2.1. It can be shown that the right hand side of (2.2) can be written in terms of the linear operator $\boldsymbol{L}$ acting on $\boldsymbol{q}$,

$$\frac{\partial \hat{\boldsymbol{q}}}{\partial t} - \boldsymbol{L}\hat{\boldsymbol{q}} = 0, \hat{\boldsymbol{q}}(0) = \boldsymbol{q}_0 \tag{2.3}$$

with the initial condition $\boldsymbol{q}_0$.
For now $\boldsymbol{L}$ is assumed to be discrete and thus $\boldsymbol{L} \in \mathbb{C}^{n\times n}$ and $\boldsymbol{q} \in \mathbb{C}^n$. By means of this simplification it is possible to show in what extent modal stability analysis fails in predicting short-term behavior of a system.

2.2 Exponential Growth

An analytical solution to (2.3) is given by

$$\hat{\boldsymbol{q}}(t) = \boldsymbol{q_0} e^{\boldsymbol{L}t}. \tag{2.4}$$

Assuming $\boldsymbol{L}$ to be diagonalisable we can write

$$\boldsymbol{L} = \boldsymbol{S}\boldsymbol{\Lambda}\boldsymbol{S}^{-1} \quad \text{with } \boldsymbol{\Lambda} := \begin{bmatrix} \lambda_1 & 0 & \dots & 0 \\ 0 & \lambda_2 & \dots & 0 \\ \ddots & \ddots & \ddots & \ddots \\ 0 & \dots & 0 & \lambda_n \end{bmatrix} \quad \text{and } \boldsymbol{S} := \begin{bmatrix} | & | & & | \\ \boldsymbol{v}_1 & \boldsymbol{v}_2 & \dots & \boldsymbol{v}_n \\ | & | & & | \end{bmatrix} \tag{2.5}$$

with λ_i eigenvalues and $\boldsymbol{v}_i$ eigenvectors of $\boldsymbol{L}$. For $t \to \infty$ the exponential term of (2.4) governs its behavior, which depends on the operator $\boldsymbol{L}$. In case $\boldsymbol{L}$ is not only diagonalisable but $\boldsymbol{S}$ has also orthonormal column vectors, such that $\boldsymbol{L}$ is normal, considering the eigenvalues would be enough to predict the long and short term behavior of the solution. That can be seen evaluating upper and lower bound of $e^{\boldsymbol{L}t}$:

$$\begin{aligned} e^{\lambda_{max} t} \leq \|e^{\boldsymbol{L}t}\| = \|\sum_{n=0}^{\infty} \frac{1}{n!}(t\boldsymbol{L})^n\| &= \|\boldsymbol{I} + t\boldsymbol{L} + \frac{t^2}{2}\boldsymbol{L}^2 + \dots\| \\ &= \|\boldsymbol{I} + t\boldsymbol{S}\boldsymbol{\Lambda}\boldsymbol{S}^{-1} + \frac{t^2}{2}(\boldsymbol{S}\boldsymbol{\Lambda}\boldsymbol{S}^{-1})(\boldsymbol{S}\boldsymbol{\Lambda}\boldsymbol{S}^{-1}) + \dots\| \\ &= \|\boldsymbol{S}(\boldsymbol{I} + t\boldsymbol{\Lambda} + \frac{t^2}{2}\boldsymbol{\Lambda}^2 + \dots)\boldsymbol{S}^{-1}\| \\ &= \|\boldsymbol{S}e^{\boldsymbol{\Lambda}t}\boldsymbol{S}^{-1}\| \leq \underbrace{\|\boldsymbol{S}\|\|\boldsymbol{S}^{-1}\|}_{=:\mathcal{K}(\boldsymbol{S})} e^{\lambda_{max} t}. \end{aligned} \tag{2.6}$$

$\mathcal{K}(\boldsymbol{S})$ is known as the condition number. If $\boldsymbol{S}$ is a normal matrix it doesn't change the length of a vector: $\|\boldsymbol{S}\boldsymbol{x}\| = \|\boldsymbol{x}\|$. The matrix norm of $\boldsymbol{S}$ and $\boldsymbol{S}^{-1}$ is then respectively

$$\|\boldsymbol{S}\| = \max_{\boldsymbol{x}\in\mathbb{C}^n \text{ with } \|\boldsymbol{x}\|=1} \|\boldsymbol{S}\boldsymbol{x}\| = 1, \tag{2.7}$$

$$\|\boldsymbol{S}^{-1}\| = \max_{\boldsymbol{y}\in\mathbb{C}^n \text{ with } \|\boldsymbol{y}\|=1} \|\boldsymbol{S}^{-1}\boldsymbol{y}\| = \max_{\boldsymbol{y}\in\mathbb{C}^n \text{ with } \|\boldsymbol{y}\|=1} \|\boldsymbol{S}^{-1}\boldsymbol{S}\boldsymbol{x}\| = 1, \tag{2.8}$$

hence the condition number is 1 and the upper and lower bound coincide. Hence, the behavior of all times is governed by the exponential term depending on λ_{max}. But in general, and often in fluid mechanics due to the convective terms, $\mathcal{K}(\boldsymbol{S}) > 1$ which means that only the asymptotic growth ($t \to \infty$) is given by the least stable mode.

In Figure 2.1 the non-orthogonal expansion of an initial condition $\boldsymbol{q_0}$ is shown in a graphical way for two dimensions. Here it becomes vividly underlined that even though v_1 and v_2 tend towards 0 for $t \to \infty$, non-orthogonal eigenvectors can give rise to short-term growth as the length of $\boldsymbol{q_0}$ on the left of the figure is actually at the third instant of time longer than at the beginning.

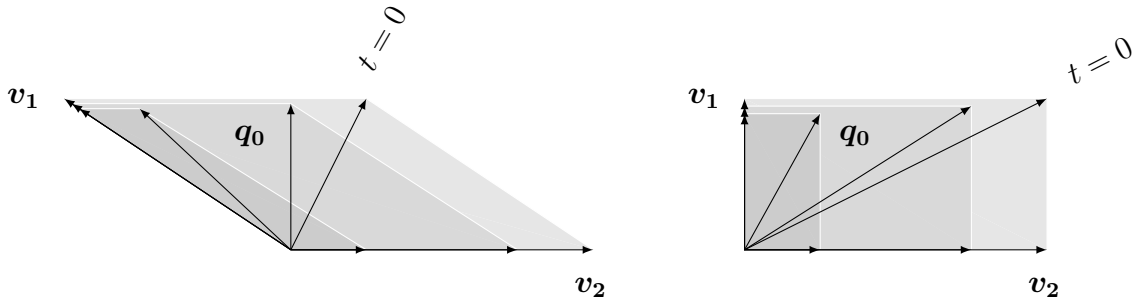

Fig. 2.1: Non-normal expansion of an initial condition $\boldsymbol{q_0}$ (left) in comparison to a normal one (right)

What actually interests is due to which initial condition $\boldsymbol{q_0}$, with $\|\boldsymbol{q_0}\| = 1$, the maximum possible perturbation $\hat{\boldsymbol{q}}$ for a certain instant in time arises. This can be described by a gain function $G(t)$ that is defined as

$$\max_{\forall \boldsymbol{q_0}} \frac{\|\hat{\boldsymbol{q}}\|}{\|\boldsymbol{q_0}\|} = \max_{\forall \boldsymbol{q_0}} \frac{\|\boldsymbol{q_0} e^{\boldsymbol{L}t}\|}{\|\boldsymbol{q_0}\|} = \|e^{\boldsymbol{L}t}\| =: G(t). \tag{2.9}$$

Here every instant in time has a corresponding unique optimal initial condition. In the simple case of a two by two matrix it can be analytically calculated using for instance the spectral norm (see example at the end of this subsection). But generally speaking this ends up in an optimization problem finding the optimal solution out of all possible initial conditions $\boldsymbol{q_0}$. Here arises the question about a meaningful measure, because the norm is what still has to be chosen in a reasonable way fitting the actual setting.

Example

Consider the following initial value problem

$$\frac{d}{dt}\begin{bmatrix} q_x \\ q_y \end{bmatrix} = \underbrace{\begin{bmatrix} \lambda_1 & p \\ 0 & \lambda_2 \end{bmatrix}}_{=:\boldsymbol{L}} \begin{bmatrix} q_x \\ q_y \end{bmatrix}, \quad \begin{bmatrix} q_x(t=0) \\ q_y(t=0) \end{bmatrix} = \begin{bmatrix} q_x^0 \\ q_y^0 \end{bmatrix}. \tag{2.10}$$

For this system the gain $G(t)$, using the spectral norm,

$$G(t) = \|e^{\boldsymbol{L}\,t}\|_{spec} = \|\boldsymbol{S}e^{\boldsymbol{\Lambda}\,t}\boldsymbol{S}^{-1}\|_{spec} = \sqrt{\lambda_{max}((\boldsymbol{S}e^{\boldsymbol{\Lambda}\,t}\boldsymbol{S}^{-1})^H(\boldsymbol{S}e^{\boldsymbol{\Lambda}\,t}\boldsymbol{S}^{-1}))} \tag{2.11}$$

has been calculated in case of stable and unstable eigenvalues and with different values for the variable p, respectively.
The gain-curves for different values of p over a time interval $t \in [0, 50]$ can be seen in Figure 2.2 and Figure 2.3. For $p = 0$ the matrix is normal showing that there is no influence of non-orthogonal eigenvectors. The behavior, recognizable by the straight line, is exponential for all times in both cases. With $p \neq 0$ this changes for both cases in a short-term sense which becomes crucial and obvious in the stable case, see Figure 2.2. The modal analysis predicts a stable and decaying solution for all times but as can be seen from the graph, for a finite time $G(t)$ is growing.

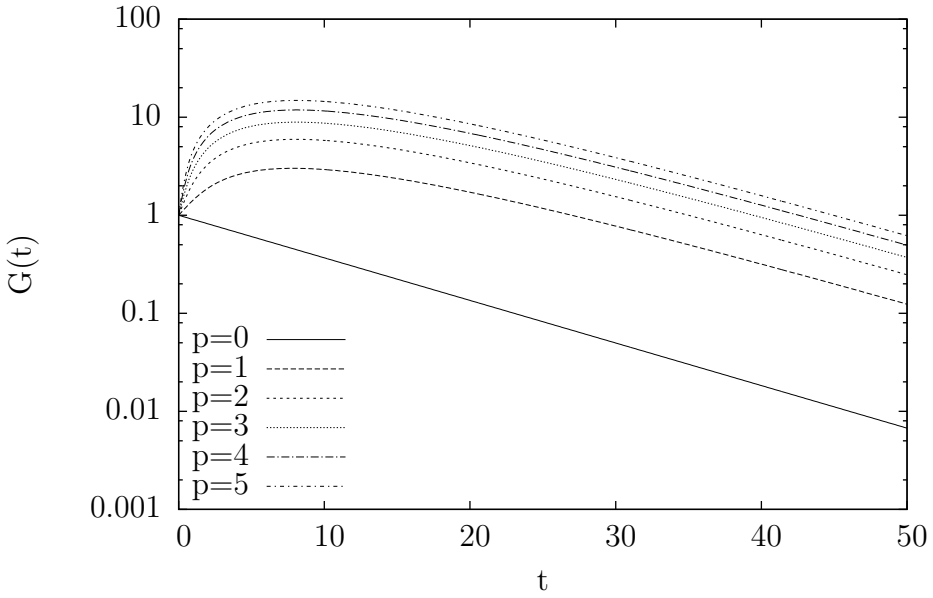

Fig. 2.2: Gain $G(t)$ for different stable $\boldsymbol{L}(p)$ with eigenvalues $\lambda_1 = -0.1$ and $\lambda_2 = -0.15$

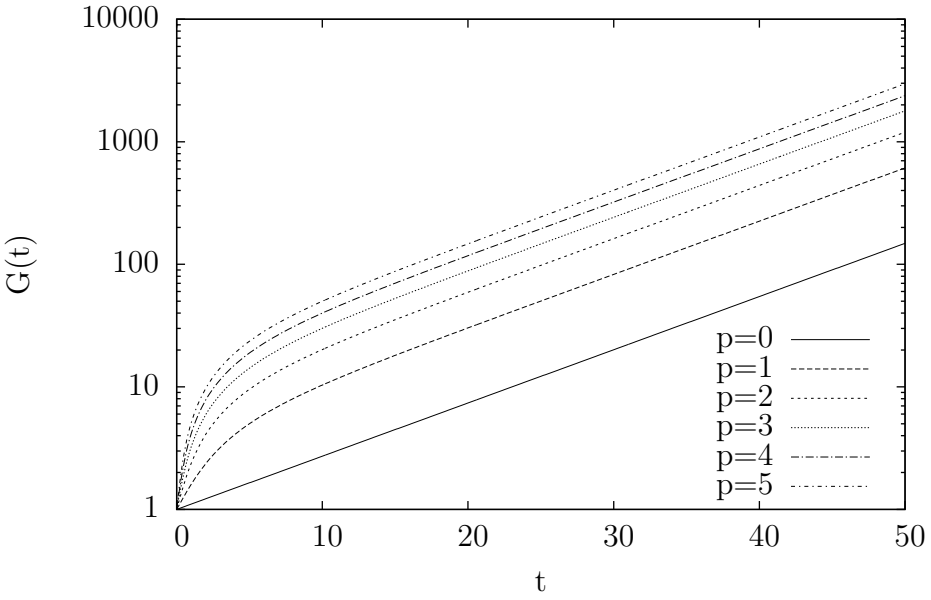

Fig. 2.3: Gain $G(t)$ for different unstable $\boldsymbol{L}(p)$ with eigenvalues $\lambda_1 = 0.1$ and $\lambda_2 = -0.15$

2.3 A More Realistic Setting

For parallel shear flows it is reasonable to consider wave-like propagating perturbations

$$\hat{\boldsymbol{q}}(\boldsymbol{x}, t) = \boldsymbol{q}(y, t) e^{i(\alpha x + \beta z)} \tag{2.12}$$

with α streamwise and β spanwise wavenumbers, respectively. The equations that govern the flow over an oscillating plate are the so called Orr-Sommerfeld equations. In chapter 3 a detailed deduction for the two-fluid case and the reformulation in terms of velocity v and normal vorticity η is given. As a disturbance measure it comes naturally to choose the kinetic energy of the flow ((Schmid, 2007, p. 134))

$$E(t) = \frac{1}{2k^2} \int_\Omega |Dv|^2 + k^2 |v|^2 + |\eta|^2 dy \tag{2.13}$$

with $k = \sqrt{\alpha^2 + \beta^2}$ and $D = \frac{\partial}{\partial y}$, which can be rewritten as a norm

$$\|\boldsymbol{q}\|^2{}_E = \frac{1}{2k^2} \int_\Omega \begin{bmatrix} v \\ \eta \end{bmatrix}^H \underbrace{\begin{bmatrix} D^2 - k^2 & 0 \\ 0 & 1 \end{bmatrix}}_{=:\boldsymbol{M}} \underbrace{\begin{bmatrix} v \\ \eta \end{bmatrix}}_{=:\boldsymbol{q}} dy = \frac{1}{2k^2} \int_\Omega \boldsymbol{q}^H \boldsymbol{M} \boldsymbol{q} dy. \tag{2.14}$$

As $\boldsymbol{M}$ is symmetric positive definite a Cholesky decomposition exists and gives $\boldsymbol{M} = \boldsymbol{T}^H \boldsymbol{T}$. With the upper triangular matrix $\boldsymbol{T}$, the energy-norm can be led back to the standard Eulerian L_2-norm:

$$\|\boldsymbol{q}\|^2{}_E = \frac{1}{2k^2} \int_\Omega \boldsymbol{q}^H \boldsymbol{M} \boldsymbol{q} dy = \frac{1}{2k^2} \int_\Omega (\boldsymbol{T}\boldsymbol{q})^H \boldsymbol{T}\boldsymbol{q} dy = \frac{1}{2k^2} \|\boldsymbol{T}\boldsymbol{q}\|^2{}_{L_2}. \tag{2.15}$$

With (2.15) and the definition (2.9), the gain in this case evolves to

$$G(t) = \max_{\forall \boldsymbol{q_0}} \frac{\|\boldsymbol{T}\boldsymbol{q}\|_{L_2}^2}{\|\boldsymbol{T}\boldsymbol{q_0}\|_{L_2}^2} = \max_{\forall \boldsymbol{q_0}} \frac{\|\boldsymbol{T}e^{\boldsymbol{L}t}\boldsymbol{q_0}\|_{L_2}^2}{\|\boldsymbol{T}\boldsymbol{q_0}\|_{L_2}^2} = \max_{\forall \boldsymbol{q_0}} \frac{\|\boldsymbol{T}e^{\boldsymbol{L}t}\boldsymbol{T}^{-1}\boldsymbol{T}\boldsymbol{q_0}\|_{L_2}^2}{\|\boldsymbol{T}\boldsymbol{q_0}\|_{L_2}^2} = \|\boldsymbol{T}e^{\boldsymbol{L}t}\boldsymbol{T}^{-1}\|_{L_2}^2. \tag{2.16}$$

$G(t)$ can be evaluated for a certain instant in time $t = T$, marching the argument in time. In case for the example in section 2.1, $G(t)$ would result similar as shown in Figure 2.2 and Figure 2.3.
In practice this is not the method of choice, as there is an inverted matrix involved and one needs to compute the eigenvalues and eigenvectors of $\boldsymbol{L}$. Instead, $G(t)$ is optimized for a certain instant in time $t = T$ over all possible initial conditions $\boldsymbol{q_0}$. From the definition in (2.9) this is a maximizing problem which can be recast in a minimizing one:

$$\min_{\forall \boldsymbol{q_0}} \frac{\|\boldsymbol{q_0}\|}{\|\boldsymbol{q}\|} \quad \text{s. t.} \quad \frac{\partial \boldsymbol{q}}{\partial t} - \boldsymbol{L}\boldsymbol{q} = \boldsymbol{0},\ 0 < t \leq T, \qquad \boldsymbol{q} = \boldsymbol{q_0},\ t = 0., \tag{2.17}$$

For every t there will be a corresponding optimal initial condition. If one wants to compute $G(t)$ using the method given by (2.17), the envelope of $\frac{\|\boldsymbol{q}\|}{\|\boldsymbol{q_0}\|}$ over different values for T must be evaluated. For the necessary optimization techniques see chapter 4.

Chapter 3

Formulation of the Mathematical Problem

In this chapter the mathematical description of the physical problem is deduced and simplified. It is shown how to get from the eye to a flat plate and how the boundary conditions are imposed for the two fluids forming an interface in between. The equations for the base flow and the perturbed flow as well as the modeling of the interface are described which result in systems of partial differential equations. Throughout this chapter * will indicate dimensional quantities.

3.1 The Eye Becomes a Flat Plate

Consider the eye as a ball filled with two immiscible and incompressible fluids as motivated in chapter 1. One fluid with density ρ_1^* covers the inner wall of the eye, another with density ρ_2^* fills up the remaining space inside the body. Keeping this in mind, some further simplifications are made in order to find solvable equations. The thickness δ^* of the fluid which separates the tamponade fluid from the retina is very small compared to the eye radius. Figure 3.1 on the right hand side shows a close up of the idealized model.

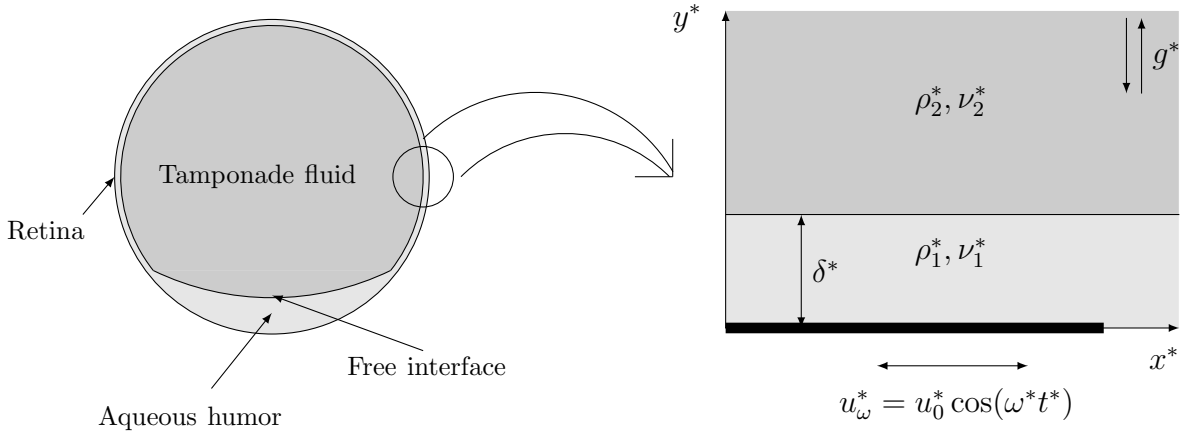

Fig. 3.1: Simplified eye with the two fluids divided by the interface (left); Close up: A wall-near area shows the actual model (right)

Here movements of the retina are assumed to behave like periodic oscillations with a no slip condition of the lower boundary. The velocity at the wall is then $u_\omega^* = u_0^* \cos(\omega^* t^*)$.

In case of a single fluid in a laminar flow at low Reynolds numbers, this is a very well studied case known as Stokes boundary layer, see for example Batchelor (2000). This case has been used for verification of the code used in this thesis, see chapter 5.

3.2 Governing Equations and Solution

The formulations are in spatial coordinates $\mathbf{x}^* = (x^*, y^*, z^*)^T$, where x^* denotes the streamwise, y^* the wall-normal and z^* the spanwise direction of the flow. Vector notation is used for convenient reading. As we assume our fluids to be incompressible, ρ_1^* and ρ_2^* will remain constant.

3.2.1 The Incompressible Navier-Stokes-Equations

The governing equations describing the behaviour of the flow are the Navier-Stokes equations for an incompressible fluid, see (3.1) and (3.2) below. They are formed by balancing the forces in a fluid due to the action of momentum

$$\rho_j^* \frac{\partial \mathbf{u}_j^*}{\partial t^*} = -\rho_j^* (\mathbf{u}_j^*, \boldsymbol{\nabla}^*)\mathbf{u}_j^* - \boldsymbol{\nabla}^* \mathbf{p}_j^* + \mu_j^* \boldsymbol{\Delta}^* \mathbf{u}_j^* + g^* \rho_j^* \boldsymbol{e}_y \tag{3.1}$$

and applying continuity of mass

$$div(\mathbf{u}_j^*) = 0, \qquad j = 1, 2. \tag{3.2}$$

$\mathbf{u}^* = (u^*, v^*, w^*)^T$ denotes the velocity vector and p^* the pressure. $\boldsymbol{\nabla}^* = (\frac{\partial}{\partial x^*}, \frac{\partial}{\partial y^*}, \frac{\partial}{\partial z^*})^T$ and $\boldsymbol{\Delta}^* \boldsymbol{u} = div(\boldsymbol{\nabla}^* \boldsymbol{u}^*) = (\boldsymbol{\nabla}^*, \boldsymbol{\nabla}^*)\boldsymbol{u}^*$ are differential operators where $(\ ,\ )$ denotes the inner product with respect to the euclidean norm. $\boldsymbol{e}_y$ denotes the unit vector in y-direction. (3.1) and (3.2) hold for both fluids, indicated by the subscripts j.

Nondimensionalization

In the specific physical problem of this thesis, the characteristic scales are the flow velocity u_0^*, the thickness of fluid 1 δ^* and its density ρ_1^*. Scaling the Navier-Stokes equations with these values and thereby removing units of the flow helps to recover significant properties and makes the results to be comparable with other flows alike. By means of dimensional analysis it can be shown that these three quantities are sufficient to form all necessary dimensions. For detailed explanations see for example Yarin (2012). The dimensional variables can then be written in terms of dimensionless variables:

$$\begin{aligned} \mathbf{x}^* &= \delta^* \mathbf{x}, & \mathbf{u}^* &= u_0^* \mathbf{u}, \\ p^* &= \rho_1^* u_0^{*2} p, & t^* &= \frac{\delta^*}{u_0^*} t, & \omega^* &= \frac{u_0^*}{\delta^*} \omega. \end{aligned} \tag{3.3}$$

Inserting these values inside (3.1) and (3.2) the new equations for the fluid on the wall, in domain Ω_1,

$$\frac{\partial \mathbf{u}_1}{\partial t} = -(\mathbf{u}_1, \boldsymbol{\nabla})\mathbf{u}_1 - \boldsymbol{\nabla} p_1 + \frac{1}{Re}\boldsymbol{\Delta}\mathbf{u}_1 + \frac{1}{Fr^2}\boldsymbol{e}_y \tag{3.4a}$$

$$div(\mathbf{u}_1) = 0 \tag{3.4b}$$

and the fluid above, in domain Ω_2,

$$\frac{\partial \mathbf{u}_2}{\partial t} = -(\mathbf{u}_2, \boldsymbol{\nabla})\mathbf{u}_2 - \frac{1}{\gamma}\boldsymbol{\nabla} p_2 + \frac{1}{Re}\frac{m}{\gamma}\boldsymbol{\Delta}\mathbf{u}_2 + \frac{1}{Fr^2}\boldsymbol{e}_y \tag{3.5a}$$

$$div(\mathbf{u}_2) = 0 \tag{3.5b}$$

are now dimensionless with the Reynolds number $Re = \frac{u_0^* \delta^* \rho_1^*}{\mu *_1}$ and the Froude number $Fr = \sqrt{\frac{u_0^* \omega^*}{g^*}}$, the fractions $\gamma = \frac{\rho_2^*}{\rho_1^*}$ and $m = \frac{\mu_2^*}{\mu_1^*}$.

3.2.2 Base Flow

As the interest lies on the evolution of small perturbations $\hat{\mathbf{u}}_j$ around a base flow $\mathbf{U}_j$ with $j = 1, 2$, the flow is written in terms of the following quantities

$$\mathbf{u}_j = \mathbf{U}_j + \hat{\mathbf{u}}_j \qquad \text{and} \qquad p_j = P_j + \hat{p}_j, \qquad j = 1, 2. \tag{3.6}$$

and results in different equations respectively. Unless stated otherwise, the following is written for fluid 1, but the equations are valid in both domains, apart from the scaling with $\frac{m}{\gamma}$ of the viscous term.
By substituting (3.6) in (3.4a) - (3.5b) and collecting the base flow terms and the perturbation terms it follows a system of equations for each fluid respectively. The base flow can be solved analytically.
Writing (3.4a) in terms of the base flow of the lower fluid will make the simplifications more understandable:

$$\frac{\partial}{\partial t}\begin{bmatrix} U_1 \\ V_1 \\ W_1 \end{bmatrix} = -\left(\begin{bmatrix} U_1 \\ V_1 \\ W_1 \end{bmatrix}, \begin{bmatrix} \frac{\partial}{\partial x} \\ \frac{\partial}{\partial y} \\ \frac{\partial}{\partial z} \end{bmatrix}\right)\begin{bmatrix} U_1 \\ V_1 \\ W_1 \end{bmatrix} - \begin{bmatrix} \frac{\partial p_1}{\partial x} \\ \frac{\partial p_1}{\partial y} \\ \frac{\partial p_1}{\partial z} \end{bmatrix} + \frac{1}{Re}\Delta\begin{bmatrix} U_1 \\ V_1 \\ W_1 \end{bmatrix} + \begin{bmatrix} 0 \\ -\frac{1}{Fr^2} \\ 0 \end{bmatrix}. \tag{3.7}$$

In case of a laminar and fully developed flow in the stream wise direction and in the limit of a parallel flow $V_1 = W_1 = 0$, the solution has the shape $\mathbf{U}_j(\mathbf{x}, t) = (U_j(y, t), 0, 0)^T, j = 1, 2$. Assuming the volume forces acting in the negative y-direction and the pressure being a function of y only, this gives

$$\frac{\partial}{\partial t}\begin{bmatrix} U_1 \\ 0 \\ 0 \end{bmatrix} = -U_1\frac{\partial}{\partial x}\begin{bmatrix} U_1 \\ 0 \\ 0 \end{bmatrix} - \begin{bmatrix} 0 \\ \frac{\partial P_1}{\partial y} \\ 0 \end{bmatrix} + \frac{1}{Re}\Delta\begin{bmatrix} U_1 \\ 0 \\ 0 \end{bmatrix} + \begin{bmatrix} 0 \\ -\frac{1}{Fr^2} \\ 0 \end{bmatrix}. \tag{3.8}$$

Finally (3.4a) simplifies to

$$\frac{\partial U_1}{\partial t} = \frac{1}{Re}\frac{\partial^2 U_1}{\partial y^2} \tag{3.9a}$$

$$\frac{\partial P_1}{\partial y} = -\frac{1}{Fr^2}, \tag{3.9b}$$

and respectively (3.5a) to

$$\frac{\partial U_2}{\partial t} = \frac{m}{\gamma}\frac{1}{Re}\frac{\partial^2 U_2}{\partial y^2} \tag{3.10a}$$

$$\frac{\partial P_2}{\partial y} = -\gamma\frac{1}{Fr^2}. \tag{3.10b}$$

The boundary and matching conditions for the base flow can be found in the schematic diagram of the two superposed fluids in Figure 3.2. The solution of (3.9a) and (3.9b) and (3.10a) and (3.10b) can be found by solving the system for each fluid separately and choosing the arising constants such that the conditions are satisfied.

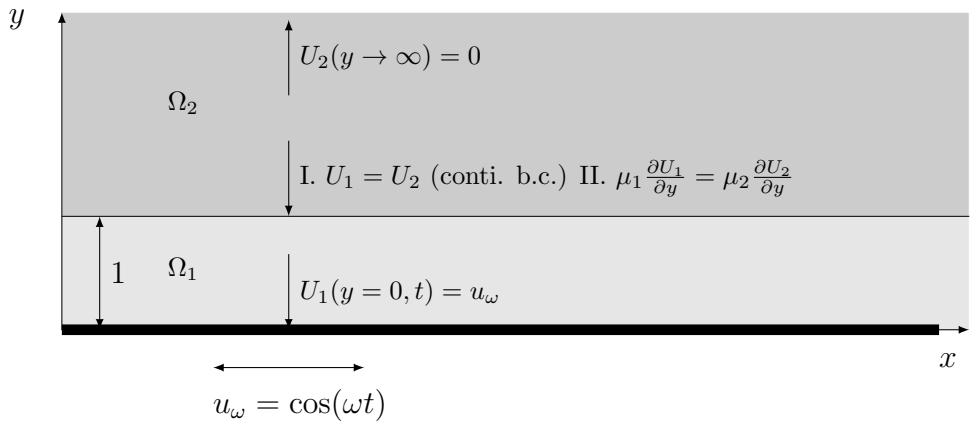

Fig. 3.2: Boundary conditions for the base flow: no-slip condition at the wall; continuity of velocity at and shear stress across the interface; vanishing velocity at infinity

Inserting the approach by (Batchelor, 2000, p. 192)

$$U_1 = \Re\{f(y)e^{-i\omega t}\} \tag{3.11}$$

into (3.9a), where $\Re$ denotes the real part, results in an ordinary differential equation $-i\omega f(y) = \frac{1}{Re}f(y)''$, where $''$ denotes the second derivative with respect to y. With its solution and $a := \sqrt{iRe\omega}$ the U_1 results in

$$\begin{aligned} U_1(y,t) &= \Re\{(c_1 e^{ay} + c_2 e^{-iay})e^{-i\omega t}\} \\ &= \Re\{(c_1 e^{ay} + c_2 e^{-iay})(\cos(\omega t) - i\sin(\omega t))\} \\ &= \frac{1}{2}(c_1 e^{ay} + c_2 e^{-ay})e^{i\omega t} + \frac{1}{2}(\bar{c_1} e^{-ay} + \bar{c_2} e^{ay})e^{-i\omega t}. \end{aligned} \tag{3.12}$$

Solving (3.10a) in the same manner leads to

$$U_2(y,t) = \Re\{(c_3 e^{by} + c_4 e^{-by})e^{-i\omega t}\}$$

with $b := \sqrt{iRe\omega\frac{m}{\gamma}}$. As $U_2 \to \infty$ for $y \to \infty$, $c_3 = 0$ is chosen.

$$U_2(y,t) = \frac{1}{2}c_4 e^{-by}e^{-i\omega t} + \frac{1}{2}\bar{c_4}e^{by}e^{-i\omega t}. \tag{3.13}$$

To determine the coefficients c_1, c_2 and c_4, the boundary conditions are applied. With the interface condition $y = 1$ follows

$$\begin{aligned} 0 &= U_1(y=1,t) - U_2(y=1,t) && (3.14)\\ &= (c_1 e^a + c_2 e^{-a})e^{i\omega t} + (\bar{c_1}e^{-ia} + \bar{c_2}e^{ia})e^{-i\omega t} - c_4 e^{-b}e^{i\omega t} - \bar{c_4}e^{b}e^{-i\omega t} \\ 0 &= \frac{\partial U_1(y=1,t)}{\partial y} - m\frac{\partial U_2(y=1,t)}{\partial y} && (3.15)\\ &= a(c_1 e^a - c_2 e^{-a})e^{i\omega t} + a(-\bar{c_1}e^{-a} + \bar{c_2}e^{a})e^{-i\omega t} - mbc_4 e^{-b}e^{i\omega t} - mb\bar{c_4}e^{b}e^{-i\omega t}. \end{aligned}$$

Applying the no-slip condition leads to

$$\begin{aligned} 0 &= U_1(y=0,t) - \frac{1}{2}(e^{i\omega t} + e^{-i\omega t}) && (3.16)\\ &= \frac{1}{2}(c_1 + c_2)e^{i\omega t} + (\bar{c_1} + \bar{c_2})e^{-i\omega t}) - \frac{1}{2}(e^{i\omega t} + e^{-i\omega t}) \\ &\Rightarrow c_1 = 1 - c_2, \bar{c_1} = 1 - \bar{c_2}. && (3.17) \end{aligned}$$

The coefficients can then be obtained as:

$$c_1 = \frac{(mb+a)e^{-a}}{(a+mb)e^{-a} + (a-mb)e^{a}} \tag{3.18a}$$

$$c_2 = \frac{(mb-a)e^{a}}{(a+mb)e^{-a} + (a-mb)e^{a}} \tag{3.18b}$$

$$c_4 = \frac{2e^{-b}}{(a+mb)e^{-a} + (a-mb)e^{a}}. \tag{3.18c}$$

With (3.12) and (3.13) expressions describing the base flow for both fluids are given.

3.2.3 Perturbed Flow

In order to reduce the number of governing equations they are written in terms of velocity $\hat{v}_1$ and normal vorticity $\hat{\eta}_1$ as presented in (Schmid and Henningson, 2000, p. 56). For the equations of the perturbed flow the perturbed and linearised Navier-Stokes equations in Ω_1

$$\frac{\partial \hat{\mathbf{u}}_1}{\partial t} = -(\hat{\mathbf{u}}_1, \boldsymbol{\nabla})\mathbf{U}_1 - (\mathbf{U}_1, \boldsymbol{\nabla})\hat{\mathbf{u}}_1 - \boldsymbol{\nabla}\hat{p}_1 + \frac{1}{Re}\Delta\hat{\mathbf{u}}_1 \tag{3.19a}$$

$$div(\hat{\mathbf{u}}_1) = 0. \tag{3.19b}$$

have to be modified. To eliminate the pressure term, (3.19a) can be written in terms of the curl $\boldsymbol{\omega}$,

$$\hat{\boldsymbol{\omega}}_1 := \boldsymbol{\nabla} \times \hat{\mathbf{u}}_1 = \begin{bmatrix} \frac{\partial \hat{w}_1}{\partial y} - \frac{\partial \hat{v}_1}{\partial z} \\ \frac{\partial \hat{u}_1}{\partial z} - \frac{\partial \hat{w}_1}{\partial x} \\ \frac{\partial \hat{v}_1}{\partial x} - \frac{\partial \hat{u}_1}{\partial y} \end{bmatrix} =: \begin{bmatrix} \hat{\xi}_1 \\ \hat{\eta}_1 \\ \hat{\nu}_1 \end{bmatrix} \tag{3.20}$$

$$\boldsymbol{\nabla} \times \mathbf{U}_1 = \begin{bmatrix} 0 \\ 0 \\ -\frac{\partial U_1}{\partial y} \end{bmatrix} \tag{3.21}$$

The second component $\hat{\eta}_1$ is the so called normal vorticity. The following identities, which result from some auxiliary calculations, are used for the conversion:

$$\frac{1}{2}\boldsymbol{\nabla}(\mathbf{u}_1, \mathbf{u}_1) = (\mathbf{u}, \boldsymbol{\nabla})\mathbf{u} + \mathbf{u} \times (\boldsymbol{\nabla} \times \mathbf{u}) \tag{3.22a}$$

$$\boldsymbol{\nabla} \times \boldsymbol{\nabla}\mathbf{u} = 0 \tag{3.22b}$$

$$(\boldsymbol{\nabla}, \boldsymbol{\omega}) = (\boldsymbol{\nabla}, \boldsymbol{\nabla} \times \mathbf{u}) = div(\boldsymbol{\nabla} \times \mathbf{u}) = 0 \tag{3.22c}$$

$$\boldsymbol{\nabla} \times (\mathbf{u} \times \boldsymbol{\omega}) = (\boldsymbol{\omega}, \boldsymbol{\nabla})\mathbf{u} - (\mathbf{u}, \boldsymbol{\nabla}) + \mathbf{u} \underbrace{(\boldsymbol{\nabla}, \boldsymbol{\omega})}_{=0 \text{ because of (3.22c)}} - \boldsymbol{\omega} \underbrace{(\boldsymbol{\nabla}, \mathbf{u})}_{=div\mathbf{u}=0} \tag{3.22d}$$

Applying first (3.22a), taking the curl on both sides and with (3.22b), (3.19a) becomes

$$\frac{\partial(\boldsymbol{\nabla} \times \hat{\mathbf{u}}_1)}{\partial t} = \boldsymbol{\nabla} \times \boldsymbol{U_1} \times \underbrace{(\boldsymbol{\nabla} \times \hat{\mathbf{u}}_1)}_{=\hat{\boldsymbol{\omega}}_1} + \boldsymbol{\nabla} \times \hat{\boldsymbol{u}}_1 \times \underbrace{(\boldsymbol{\nabla} \times \mathbf{U}_1)}_{=\hat{\boldsymbol{\Omega}}_1} + \frac{1}{Re}\boldsymbol{\Delta} \underbrace{(\boldsymbol{\nabla} \times \hat{\mathbf{u}}_1)}_{=\hat{\boldsymbol{\omega}}_1}. \tag{3.23}$$

With (3.22c) the second component of (3.23) gives the equation for η_1. For the eliminated pressure an additional relation is needed. Like proposed in (Schmid and Henningson, 2000, p. 55) the perturbation pressure can be written as

$$\nabla^2 \hat{p}_1 = -2\frac{\partial U_1}{\partial y}\frac{\partial \hat{v}_1}{\partial x}. \tag{3.24}$$

This follows after taking the divergence of (3.19a) and substituting (3.19b).
For convenience ∇ and ∇^2 are introduced as a short form of $\nabla = \frac{\partial}{\partial x} + \frac{\partial}{\partial y} + \frac{\partial}{\partial z}$ and $\nabla^2 = \frac{\partial^2}{\partial x^2} + \frac{\partial^2}{\partial y^2} + \frac{\partial^2}{\partial z^2}$ from the definition of $\boldsymbol{\Delta} = (\nabla^2, \nabla^2, \nabla^2)^T$.
With (3.24) in the second component of the linearized perturbed momentum equation and applying ∇^2, the equations for $\hat{v}_1$ and η_1 follow

$$(\frac{\partial}{\partial t} + U_1\frac{\partial}{\partial x})\nabla^2 \hat{v}_1 = \frac{\partial^2 U_1}{\partial y^2}\frac{\partial \hat{v}_1}{\partial x} + \frac{1}{Re}\nabla^4 \hat{v}_1 \tag{3.25a}$$

$$\frac{\partial \hat{\eta}_1}{\partial t} = -U_1\frac{\partial \hat{\eta}_1}{\partial x} - \frac{\partial U_1}{\partial y}\frac{\partial \hat{v}_1}{\partial z} + \frac{1}{Re}\Delta\hat{\eta}_1. \tag{3.25b}$$

The governing equations in Ω_2 can be achieved in the same way:

$$(\frac{\partial}{\partial t} + U_2\frac{\partial}{\partial x})\nabla^2 \hat{v}_2 = \frac{1}{\gamma}\frac{\partial^2 U_2}{\partial y^2}\frac{\partial \hat{v}_2}{\partial x} + \frac{1}{Re}\frac{m}{\gamma}\nabla^4 \hat{v}_2 \tag{3.26a}$$

$$\frac{\partial \hat{\eta}_2}{\partial t} = -U_2\frac{\partial \hat{\eta}_2}{\partial x} - \frac{\partial U_2}{\partial y}\frac{\partial \hat{v}_2}{\partial z} + \frac{1}{Re}\frac{m}{\gamma}\Delta\hat{\eta}_2. \tag{3.26b}$$

Fourier Expansion

As in Schmid and Henningson (2000) assumed, the perturbation variables behave like waves in the x-z plane with α streamwise and β spanwise wave number, respectively. The expansion in Fourier modes are the following

$$\hat{u}_{1/2} = u(y,t)e^{i(\alpha x+\beta z)} + c_c \tag{3.27a}$$
$$\hat{v}_{1/2} = v(y,t)e^{i(\alpha x+\beta z)} + c_c \tag{3.27b}$$
$$\hat{w}_{1/2} = w(y,t)e^{i(\alpha x+\beta z)} + c_c \tag{3.27c}$$
$$\hat{p}_{1/2} = p(y,t)e^{i(\alpha x+\beta z)} + c_c \tag{3.27d}$$
$$\hat{\eta}_{1/2} = \eta(y,t)e^{i(\alpha x+\beta z)} + c_c, \tag{3.27e}$$

c_c denoting the complex conjugate. With (3.27a)-(3.27e) and

$$\nabla^2\hat{\eta} = \frac{\partial^2\hat{\eta}}{\partial^2 y} + (i\alpha)^2\hat{\eta} + (i\beta)^2\hat{\eta} = \underbrace{\frac{\partial^2\hat{\eta}}{\partial y^2}}_{=:D^2\hat{\eta}} - \underbrace{(\alpha^2+\beta^2)}_{=:k^2}\hat{\eta}$$

the equations simplify for both fluids to the so called Orr-Sommerfeld equations

$$\frac{\partial}{\partial t}(D^2-k^2)v_1 = \left[i\alpha\frac{\partial^2 U_1}{\partial y^2} - i\alpha U_1(D^2-k^2) + \frac{1}{Re}(D^2-k^2)^2\right]v_1 \tag{3.28a}$$
$$\frac{\partial\eta_1}{\partial t} = \left[-i\alpha U_1 + \frac{1}{Re}(D^2-k^2)\right]\eta_1 - i\beta\frac{\partial U_1}{\partial y}v_1, \tag{3.28b}$$

$$\frac{\partial}{\partial t}(D^2-k^2)v_2 = \left[i\alpha\frac{\partial^2 U_2}{\partial y^2} - i\alpha U_2(D^2-k^2) + \frac{1}{Re}\frac{m}{\gamma}(D^2-k^2)^2\right]v_2 \tag{3.29a}$$
$$\frac{\partial\eta_2}{\partial t} = \left[-i\alpha U_2 + \frac{1}{Re}\frac{m}{\gamma}(D^2-k^2)\right]\eta_2 - i\beta\frac{\partial U_2}{\partial y}v_2. \tag{3.29b}$$

3.2.4 Two-Fluid Interface

The theory and conditions for the interface presented here can be found in (Joseph and Renardy, 1993, p. 25 et seqq.). On the interface continuity of velocities, the kinematic condition and continuity of shear stress have to be fulfilled and the jump in normal stress has to be balanced by the surface tension. An overview on the boundary conditions can be seen in Figure 3.4.

It is necessary to introduce a new variable ξ, the deviation of the interface from its resting position at $y = 1$, see Figure 3.3. From now on one has to carefully distinguish between values at $y = 1$ and $y = 1 + \xi$, which are exactly at the surface and denoted with $^{\xi}$.

A first order linearisation of the velocity on the interface is given by

$$\boldsymbol{u}(y = 1+\xi) = \boldsymbol{u}^{\xi} = \boldsymbol{u}(y=1) + \xi\frac{\partial \boldsymbol{U}}{\partial y} = \boldsymbol{u} + \xi\boldsymbol{U}'. \tag{3.30}$$

$'$ denotes further on the derivative with respect to y.

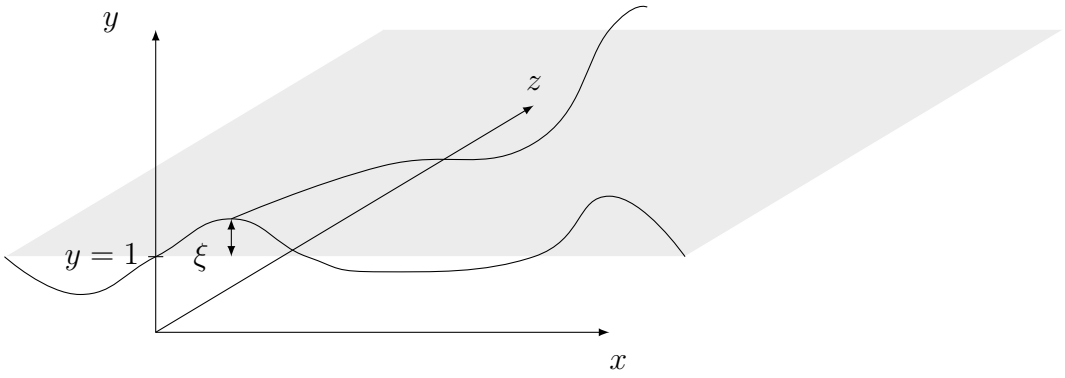

Fig. 3.3: Resting interface at $y = 1$ with curves on the deviated interface in $y - z$ and $y - x$ plane for illustrating $\xi = \xi(t, x, z)$

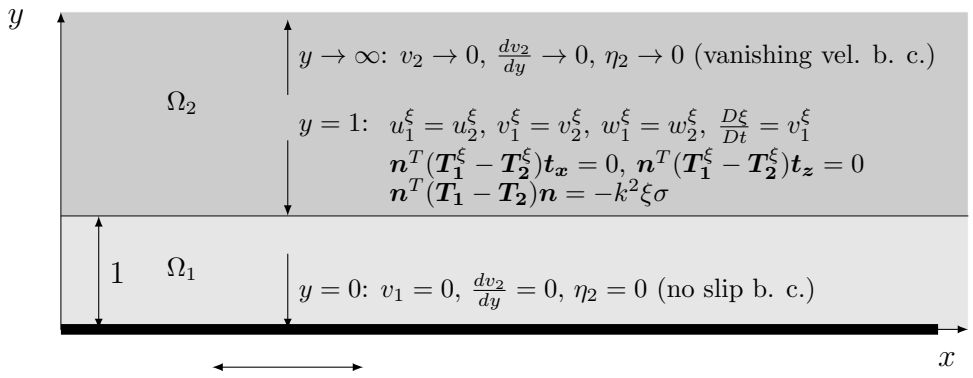

Fig. 3.4: Boundary conditions for the perturbed flow

Continuity of Velocity and Kinematic Condition

For continuity of velocity on the interface it follows, with the base flow $V_1 = W_1 = 0$ that

$$u_1^\xi = u_2^\xi \tag{3.31a}$$
$$v_1^\xi = v_2^\xi \quad \Rightarrow v_1 = v_2 \tag{3.31b}$$
$$w_1^\xi = w_2^\xi \quad \Rightarrow w_1 = w_2. \tag{3.31c}$$

Using (3.31a) - (3.31c) in the definition of normal vorticity η at $y = 1$ and formulating this by using linearized velocities, the following holds

$$\begin{aligned} \eta_1 + \frac{\partial w_1}{\partial x} - \frac{\partial u_1}{\partial z} &= \eta_2 + \frac{\partial w_2}{\partial x} - \frac{\partial u_2}{\partial z} \\ \eta_1 + i\alpha w_1 - i\beta(u_1^\xi - \xi U_1) &= \eta_2 + i\alpha w_2 - i\beta(u_2^\xi - \xi U_2) \\ \Rightarrow \eta_1 + i\beta\xi U_1 &= \eta_2 + i\beta\xi U_2. \end{aligned} \tag{3.32}$$

Similarly, the last equation for continuity of velocity in terms of v and η can be deduced

from the continuity equation at $y = 1$

$$\begin{aligned}\frac{\partial u_1}{\partial x} + \frac{\partial v_1}{\partial y} + \frac{\partial w_1}{\partial z} &= \frac{\partial u_2}{\partial x} + \frac{\partial v_2}{\partial y} + \frac{\partial w_2}{\partial z} \\ i\alpha(u_1 + \xi U_2') + v_1' + i\beta w_1 &= i\alpha(u_2 - \xi U_2') + v_2' + i\beta w_2 \\ \Rightarrow v_1' - i\alpha\xi U_1' &= v_2' - i\alpha\xi U_2'. \end{aligned} \tag{3.33}$$

Furthermore it is required, that the material derivative of the interface deviation is equal to the velocity in y-direction at the interface:

$$\frac{D\xi}{Dt} = \frac{\partial \xi}{\partial t} + \frac{\partial x}{\partial t}\frac{\partial \xi}{\partial x} = \frac{\partial \xi}{\partial t} + i\alpha\xi U_1 = v_1^\xi = v_1. \tag{3.34}$$

Continuity of Stress

The stress balance equation, which can be found in (Joseph and Renardy, 1993, p. 23), reads in the present case

$$(\boldsymbol{T}_1^\xi - \boldsymbol{T}_2^\xi)\boldsymbol{n} = \nabla_\parallel \sigma + 2H\sigma\boldsymbol{n} \tag{3.35}$$

with $\boldsymbol{n}$ the outer normal vector such that $\boldsymbol{n} = \boldsymbol{n}_1 = \boldsymbol{n}_2$. H represents the mean curvature, σ the surface tension, $\nabla_\parallel = \boldsymbol{\nabla} - \boldsymbol{n}(\boldsymbol{n}, \boldsymbol{\nabla})$ the surface gradient and $\boldsymbol{T}_j^\xi$, $j = 1, 2$ the stress tensors at the interface. Then

$$\begin{aligned}\boldsymbol{T}_j^\xi &= -p_j^\xi \boldsymbol{I} + \mu_j^*(\nabla \boldsymbol{u}_j^\xi + (\nabla \boldsymbol{u}_j^\xi)^T) \\ &= \begin{bmatrix} p_j^\xi & 0 & 0 \\ 0 & p_j^\xi & 0 \\ 0 & 0 & p_j^\xi \end{bmatrix} - \mu_j^* \underbrace{\begin{bmatrix} 2\frac{\partial u_j^\xi}{\partial x} & \frac{\partial u_j^\xi}{\partial y} + \frac{\partial v_j^\xi}{\partial x} & \frac{\partial u_j^\xi}{\partial z} + \frac{\partial w_j^\xi}{\partial x} \\ \text{sym.} & 2\frac{\partial v_j^\xi}{\partial y} & \frac{\partial v_j^\xi}{\partial z} + \frac{\partial w_j^\xi}{\partial y} \\ \text{sym.} & \text{sym.} & 2\frac{\partial w_j^\xi}{\partial z} \end{bmatrix}}_{=:\tau_j} \\ &= \begin{bmatrix} p_j & 0 & 0 \\ 0 & p_j & 0 \\ 0 & 0 & p_j \end{bmatrix} - \mu_j^* \begin{bmatrix} 2i\alpha(u_j + \xi U_j') & u_j' + \xi U_j'' + i\alpha v_j & i\beta(u_j + \xi U_j') + i\alpha w_j \\ \text{sym.} & 2v_j' & i\beta v_j + w_j' \\ \text{sym.} & \text{sym.} & 2i\beta w_j \end{bmatrix}. \end{aligned} \tag{3.36}$$

The normalized tangential and normal directions are

$$\boldsymbol{t}_1 = \frac{1}{\sqrt{1 + (\frac{\partial \xi}{\partial x})^2}} \begin{bmatrix} 1 \\ 0 \\ \frac{\partial \xi}{\partial x} \end{bmatrix}, \quad \boldsymbol{t}_2 = \frac{1}{\sqrt{1 + (\frac{\partial \xi}{\partial z})^2}} \begin{bmatrix} \frac{\partial \xi}{\partial z} \\ 0 \\ 1 \end{bmatrix}, \quad \boldsymbol{n} = \frac{1}{\sqrt{1 + (\frac{\partial \xi}{\partial x})^2 + (\frac{\partial \xi}{\partial z})^2}} \begin{bmatrix} \frac{\partial \xi}{\partial x} \\ 1 \\ \frac{\partial \xi}{\partial z} \end{bmatrix}. \tag{3.37}$$

For simplification, only the linear terms are taken into account, which coincides with assuming $\boldsymbol{t}_1 = \boldsymbol{e}_x$, $\boldsymbol{t}_2 = \boldsymbol{e}_z$ and $\boldsymbol{n} = \boldsymbol{e}_y$ for the left hand side. The nonlinearities can be found in (Joseph and Renardy, 1993, p. 185). The right hand side then simplifies to

$$\nabla_\parallel \sigma + 2H\sigma\boldsymbol{n} = \begin{bmatrix} \frac{\partial \sigma}{\partial x} \\ 0 \\ \frac{\partial \sigma}{\partial z} \end{bmatrix} + \begin{bmatrix} 0 \\ 2\frac{(\frac{\partial^2 \xi}{\partial x^2} + \frac{\partial^2 \xi}{\partial z^2})}{2}\sigma \\ 0 \end{bmatrix}. \tag{3.38}$$

In this work, the surface tension is a constant which leads to the tangential traction being continuous:

$$\boldsymbol{t}_l(\boldsymbol{T}_1^{\xi} - \boldsymbol{T}_2^{\xi})\boldsymbol{n} = 0, \quad l = 1, 2. \tag{3.39}$$

The jump in the normal stress is balanced by surface tension:

$$\boldsymbol{n}(\boldsymbol{T}_1^{\xi} - \boldsymbol{T}_2^{\xi})\boldsymbol{n} = -k^2\xi\sigma^*\boldsymbol{n}. \tag{3.40}$$

The equations for the tangential stresses then follow

$$\mu_1^*(u_1' + \xi U_1'' + i\alpha v_1) = \mu_2^*(u_2' + \xi U_2'' + i\alpha v_2) \tag{3.41a}$$

$$\mu_1^*(i\beta v_1 + w_1') = \mu_2^*(i\beta v_2 + w_2'). \tag{3.41b}$$

In order to write (3.41a) and (3.41b) in terms of v and η, the derivative with respect to y of mass-continuity ((3.4b) and (3.5b)) and some algebra is necessary:

$$\begin{aligned}
&\frac{\partial}{\partial y}(i\alpha u_1 + v_1' + i\beta w_1 = m(i\alpha u_2 + v_2' + i\beta w_2)) \\
&- \qquad i\beta((i\beta v_1 + w_1') = m(i\beta v_2 + w_2')) \\
&\hline
&i\alpha u_1' + v_1'' + \beta^2 v_1 = m(i\alpha u_2' + v_2'' + \beta^2 v_2) \\
&- \qquad i\alpha(u_1' + \xi U_1'' + i\alpha v_1 = m(u_2' + \xi U_2'' + i\alpha v_2)) \\
&\hline
&-i\alpha\xi U_1'' + k^2 v_1 + v_1'' = m(-i\alpha\xi U_2'' + k^2 v_2 + v_2'')
\end{aligned} \tag{3.42}$$

$$\begin{aligned}
&i\beta({}_1(u_1' + \xi U_1'' + i\alpha v_1) = m(u_2' + \xi U_2'' + i\alpha v_2)) \\
&- \qquad i\alpha(i\beta v_1 + w_1' = m(i\beta v_2 + w_2')) \\
&\hline
&i\beta u_1' - i\alpha w_1' + i\beta\xi U_1'' = m(i\beta u_2' - i\alpha w_2' + i\beta\xi U_2'') \\
&\Rightarrow \eta_1' + i\beta\xi U_1'' = m(\eta_2' + i\beta\xi U_2'')
\end{aligned} \tag{3.43}$$

In the condition for the normal stress, the pressure on the surface has to be defined, because the deviation of the surface ξ contributes to the hydrostatic pressure. The non-dimensional equation (3.44) then follow as

$$\begin{aligned}
{p_1^*}^{\xi} - {p_2^*}^{\xi} + 2{\mu_1}^* {v_1'}^* - 2{\mu_2}^* {v_2'}^* &= -k^2\xi\sigma^* \\
\frac{\rho_1^*}{\rho_1^*}p_1 + \frac{\rho_1^*\delta^* g^*\xi}{\rho_1^* {u_0^*}^2} - \frac{\rho_2^*}{\rho_1^*}p_2 - \frac{\rho_2^* g^*\delta^*\xi}{\rho_1^* {u_0^*}^2} + 2\frac{\mu_1^*}{\mu_1^*}v_1' - 2\frac{\mu_2^*}{\mu_1^*}v_2' &= -\frac{\sigma^*}{\rho_1^*\delta^* {u_0^*}^2}k^2\xi \\
p_1 - \gamma p_2 + 2v_1' - 2mv_2' &= -\sigma k^2\xi - \frac{\xi(1-\gamma)}{Fr^2}.
\end{aligned} \tag{3.44}$$

The pressure can be substituted from the linearized Navier-Stokes-equation for the perturbed velocities after applying ∇ on it. By multiplying (3.44) with k^2 and using (3.24) for the perturbed pressure, it follows

$$\begin{aligned} -k^2 p_1 + p_1'' &= -k^2 p_1 - i\alpha(U_1' v_1 + U_1 v_1') + \frac{1}{Re}(-k^2 v_1' + v_1''') - \frac{\partial v_1'}{\partial t} \\ &= -2i\alpha U_1' v_1 \end{aligned} \tag{3.45}$$

$$\Rightarrow k^2 p_1 = i\alpha(U_1' v_1 - U_1 v_1') + \frac{1}{Re}(-k^2 v_1' + v_1''') - \frac{\partial v_1'}{\partial t} \tag{3.46}$$

$$\begin{aligned} \frac{1}{\gamma}(-k^2 p_2 + p_2'') &= \frac{1}{\gamma}(-k^2 p_2 + i\alpha(U_2' v_2 + U_2 v_2') - \frac{1}{Re}\frac{m}{\gamma}(-k^2 v_2' + v_2''') - \frac{\partial v_2'}{\partial t}) \\ &= \frac{1}{\gamma}(-2i\alpha U_1' v_1) \end{aligned}$$

$$\Rightarrow k^2 p_2 = i\alpha(U_2' v_2 - U_2 v_2') + \frac{1}{Re}\frac{m}{\gamma}(-k^2 v_2' + v_2''') - \frac{\partial v_2'}{\partial t} \tag{3.47}$$

which gives, after inserting in (3.44), the following condition:

$$\begin{aligned} &i\alpha(U_1' v_1 - U_1 v_1') + \frac{1}{Re}(-k^2 v_1' + v_1''') - \frac{\partial v_1'}{\partial t} \\ &\quad - \left[i\alpha\gamma(U_2' v_2 - U_2 v_2') + \frac{1}{Re} m(-k^2 v_2' + v_2''') - \gamma\frac{\partial v_2'}{\partial t} \right] \\ &\quad = -\sigma k^4 \xi - \frac{k^2(1-\gamma)}{Fr^2}\xi. \end{aligned} \tag{3.48}$$

Finally with (3.31b), (3.32), (3.33), (3.34), (3.42), (3.43) and (3.48) all conditions which have to hold on the interface are specified.

3.2.5 Resulting System

The governing equations for both domains, Ω_1 and Ω_2, (3.28a), (3.28b), (3.29a) and (3.29b) can be presented as one system respectively:

$$\underbrace{\begin{bmatrix} -D^2 + k^2 & 0 \\ 0 & 1 \end{bmatrix}}_{=:\boldsymbol{B}_1} \frac{\partial}{\partial t} \underbrace{\begin{bmatrix} v_1 \\ \eta_1 \end{bmatrix}}_{=:\boldsymbol{q}_1} + \underbrace{\begin{bmatrix} A_{11}^1 & 0 \\ i\beta U_1' & A_{22}^1 \end{bmatrix}}_{=:\boldsymbol{A}_1} \begin{bmatrix} v_1 \\ \eta_1 \end{bmatrix} = \begin{bmatrix} 0 \\ 0 \end{bmatrix}, \text{ in } \Omega_1 \tag{3.49}$$

$$\underbrace{\begin{bmatrix} -D^2 + k^2 & 0 \\ 0 & 1 \end{bmatrix}}_{=:\boldsymbol{B}_2} \frac{\partial}{\partial t} \underbrace{\begin{bmatrix} v_2 \\ \eta_2 \end{bmatrix}}_{=:\boldsymbol{q}_2} + \underbrace{\begin{bmatrix} A_{11}^2 & 0 \\ i\beta U_2' & A_{22}^2 \end{bmatrix}}_{=:\boldsymbol{A}_2} \begin{bmatrix} v_2 \\ \eta_2 \end{bmatrix} = \begin{bmatrix} 0 \\ 0 \end{bmatrix}, \text{ in } \Omega_2 \tag{3.50}$$

with the following coefficients

$$A_{11}^1 := i\alpha U_1'' - i\alpha U_1(D^2 - k^2) + \frac{1}{Re}(D^2 - k^2)^2 \tag{3.51a}$$

$$A_{22}^1 := -i\alpha U_1 + \frac{1}{Re}(D^2 - k^2) \tag{3.51b}$$

$$A_{11}^2 := i\alpha U_2'' - i\alpha U_2(D^2 - k^2) + \frac{1}{Re}\frac{m}{\gamma}(D^2 - k^2)^2 \tag{3.51c}$$

$$A_{22}^2 := -i\alpha U_2 + \frac{1}{Re}\frac{m}{\gamma}(D^2 - k^2). \tag{3.51d}$$

3.3 A Disturbance Growth Measure

In order to find the worst case scenario a disturbance measure is needed for which one part is the kinetic energy of both flows, but in this case also the energy of the interface comes into account. The work in (Orazzo et al., 2014, p. 49 et seq.) proposed for a similar case an energy norm, divided in flow E_q and interface energy E_ξ, that reads in terms of v and η

$$\begin{aligned} E(t) := E_q(t) + E_\xi(t) =& \frac{1}{2k^2}\int_0^1 |Dv_1|^2 + k^2|v_1|^2 + |\eta_1|^2 dy \\ &+ \frac{1}{2k^2}\int_1^{y_{max}} |Dv_2|^2 + k^2|v_2|^2 + |\eta_2|^2 dy \\ &+ \frac{1}{2}\frac{S\,k^2}{Re^2}|\xi|^2. \end{aligned} \tag{3.52}$$

The first two integrals form E_q and can be written as an inner product with $\boldsymbol{M}$ being symmetric positive definite,

$$\begin{aligned} E_q = \|\boldsymbol{q}\|_E^2 =& \frac{1}{2k^2}\int_0^{y_{max}} \begin{bmatrix} v_1 \\ \eta_1 \\ v_2 \\ \eta_2 \end{bmatrix}^H \underbrace{\begin{bmatrix} D^2 - k^2 & 0 & 0 & 0 \\ 0 & 1 & 0 & 0 \\ 0 & 0 & D^2 - k^2 & 0 \\ 0 & 0 & 0 & 1 \end{bmatrix}}_{=:\boldsymbol{M}} \underbrace{\begin{bmatrix} v_1 \\ \eta_1 \\ v_2 \\ \eta_2 \end{bmatrix}}_{=:\boldsymbol{q}} dy \\ =& \frac{1}{2k^2}\int_0^{y_{max}} \boldsymbol{q}^H \boldsymbol{M}\boldsymbol{q} dy =: \frac{1}{2k^2}(\boldsymbol{q},\boldsymbol{q})_{\boldsymbol{M}} \end{aligned} \tag{3.53}$$

The formulation in terms of an $\boldsymbol{M}$-scalar product $(\ ,\ )_{\boldsymbol{M}}$ will be helpful in chapter 4 for the deduction of the continuous optimality conditions.

Chapter 4

Optimization

In order to formulate a solution procedure for the continuous optimality problem resulting from the equations established in chapter 3 and with the theory from chapter 2, the governing equations need to be discretized. There are two methods, either *first discretize, then optimize* or *first optimize, then discretize*. Both approaches have been implemented and will be described below. For the deduction of the optimality conditions and the adjoint system the Lagrange formalism has been applied.
An extensive discussion of existence and uniqueness of the solution shall not be made here. For further understanding Hinze et al. (2008) provides a good lecture on optimization with PDE constraints. All necessary preconditions for a unique solution are supposed to be fulfilled.

The continuous optimization problem is specified in the following way

$$\begin{aligned}
\min_{\boldsymbol{q}_0 \neq 0} J(T) \qquad s.t. \qquad & \boldsymbol{B}_1 \frac{\partial \boldsymbol{q}_1}{\partial t} + \boldsymbol{A}_1 \boldsymbol{q}_1 = \boldsymbol{0}, \boldsymbol{q}_1 \in \Omega_1,\ 0 < t \leq T, \\
& \boldsymbol{B}_2 \frac{\partial \boldsymbol{q}_2}{\partial t} + \boldsymbol{A}_2 \boldsymbol{q}_2 = \boldsymbol{0}, \boldsymbol{q}_2 \in \Omega_2,\ 0 < t \leq T, \\
& \boldsymbol{q}(\boldsymbol{x}, 0) = \boldsymbol{q}_0,\ \boldsymbol{q} \in \Omega,\ \ t = 0, \\
& \boldsymbol{q}_1(y, t) = \boldsymbol{q}_W,\ y = 0,\ \ 0 < t \leq T, \\
& \boldsymbol{q}_2(y, t) = \boldsymbol{q}_I,\ y \to \infty,\ \ 0 < t \leq T, \\
& \boldsymbol{q}(y, t) = \boldsymbol{q}_S,\ y = 1 + \xi,\ 0 < t \leq T.
\end{aligned} \tag{4.1}$$

The cost functional $J(T) := \frac{E_q(0)+E_\xi(0)}{E_q(T)+E_\xi(T)}$ is minimized subject to $(s.t.)$ the initial boundary value problem with (3.49) and (3.50) in the domain $\Omega := \Omega_1 \cup \Omega_2$, where the energy at time T depends on the solution $\boldsymbol{q}$ at final time $t = T$: $E(T) = E(\boldsymbol{q}(T))$. Instead of maximizing the energy over all possible initial conditions $\boldsymbol{q}_0$, normalized by the initial energy at $t = 0$, the inverse is minimized. The boundary conditions $\boldsymbol{q}_W$ and $\boldsymbol{q}_I$ are specified at the wall and for $y \to \infty$. The conditions on the interface $y = 1+\xi$ are summarized in $\boldsymbol{q}_S$.

4.1 Discretization

The chosen discretization is applied to both approaches. For the spatial discretization of $\Omega = \Omega_1 \oplus \Omega_2$ an equally spaced grid from $y = 0$ to y_{max} is chosen with the step size

$\delta y = \frac{y_S}{n_{y1}}$, where $y_S = 1$ and n_{y1} is the number of steps between wall and interface, see Figure 4.1.

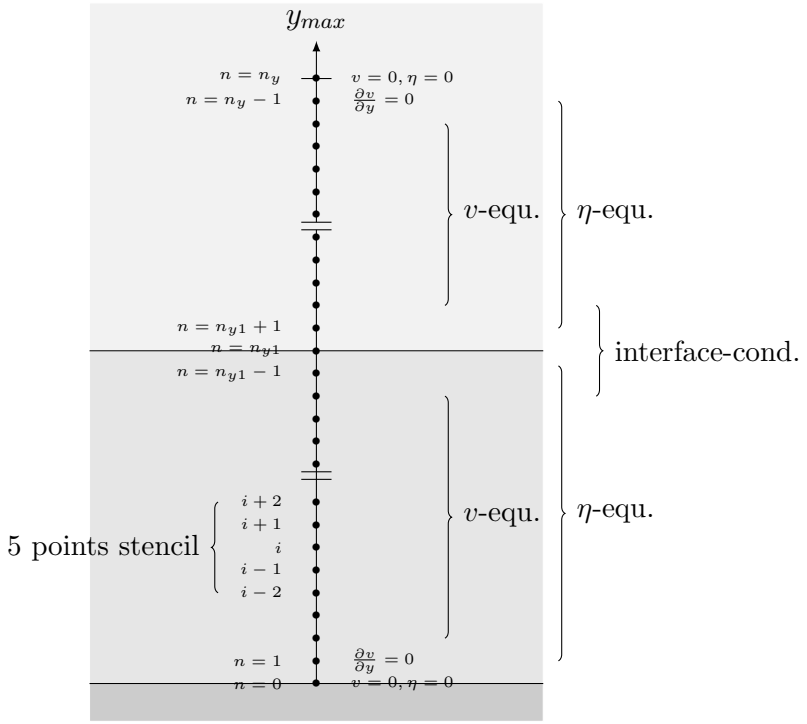

Fig. 4.1: Spatial discretization for two fluids with boundary conditions and interface

The η-equations are implemented for $n \in \{1, ..., n_{y1} - 1, n_{y1} + 1, ..., n_y - 1\}$ as there is only a second derivative involved, but in the v-equations there is a fourth derivative to specify and therefore it is written for $n \in \{2, ..., n_{y1} - 2, n_{y1} + 2, ..., n_y - 2\}$. In the latter case there is a five-point stencil necessary in order to achieve overall accuracy of second order. At the interface there is at maximum a discretization of a third derivative needed. Since the interface conditions implemented in one domain cannot include quantities from the other domain respectively, backward and forward schemes are necessary. The discrete derivatives chosen can be seen in Table 4.1. The coefficients for the backward differences

Tab. 4.1: Discrete central derivatives with second order of accuracy for all grades necessary

	central	forward
$v'(y_i)$	$\frac{1}{h}(-0.5v^{i-1} + 0.5v^{i+1})$	$\frac{1}{h}(-1.5v^i + 2v^{i+1} - 0.5v^{i+2})$
$v''(y_i)$	$\frac{1}{h^2}(v^{i-1} - 2v^i + v^{i+1})$	$\frac{1}{h^2}(2v^i - 5v^{i+1} + 4v^{i+2} - v^{i+3})$
$v'''(y_i)$	-	$\frac{1}{h^3}(-2.5v^i + 9v^{i+1} - 12v^{i+2} + 7v^{i+3} - 1.5v^{i+4})$
$v''''(y_i)$	$\frac{1}{h^4}(v^{i-2} - 4v^{i-1} + 6v^i - 4v^{i+1} + v^{i+2})$	-

are symmetric to the once of the forward scheme with negative sign for uneven derivatives.

For the time discretization the three-step Adams-Bashfordth and the two-step Crank-Nicolson method were tested.

4.2 First Discretized, Then Optimized

After spatial discretization, indicated by the ^{d}, of (4.1) with the specified discretization schemes from section 4.1, the discrete problem reads

$$\min_{\boldsymbol{q}_0{}^d \neq 0} J^d(T) \qquad s.t. \qquad \boldsymbol{B}^d \frac{\partial \boldsymbol{q}^d}{\partial t} + \boldsymbol{A}^d \boldsymbol{q}^d = \boldsymbol{0}, \boldsymbol{q}^d \in \Omega^d,\ 0 < t \leq T \tag{4.2}$$
$$\boldsymbol{q}^d = \boldsymbol{q}_0{}^d, \boldsymbol{q}^d \in \Omega^d,\ t = 0.$$

Here the two systems for each domain are written in one system also including the boundary conditions and the interface variable ξ.

4.2.1 Discrete Cost Functional

The discrete cost-functional evolves to

$$J^d(T) = \frac{E^d(\mathbf{q}^d(t=0))}{E^d(\mathbf{q}^d(t=T))} = \frac{\boldsymbol{q}_0{}^{dH} \mathbf{M}^d \boldsymbol{q}_0{}^d}{\mathbf{q}^d(T)^H \mathbf{M}^d \boldsymbol{q}^d(T)} \tag{4.3}$$

because the energy can be written as a discrete sum

$$E(t) \approx \frac{1}{2k^2} \mathbf{q}^d(t)^H \mathbf{M}^d \boldsymbol{q}^d(t) \delta y =: E^d(t). \tag{4.4}$$

Here $\boldsymbol{M}^d$ denotes the discrete version of the matrix from section 3.3. For convenience ξ^d is also included in $\boldsymbol{q}^d$ and $\boldsymbol{M}^d$ is manipulated with adding one line and column at the interface ($n = n_{y1}$) and the coefficient $m_{n_{y1},n_{y1}} = \frac{Sk^4}{Re^2}$.

4.2.2 Optimality Conditions

With the Lagrange function it is possible to write the constrained optimization problem in terms of one function

$$\begin{aligned}\mathcal{L}^d(\boldsymbol{q}^d(t), \boldsymbol{q}_0{}^d, \boldsymbol{a}^d, \boldsymbol{b}^d) =& \frac{\boldsymbol{q}_0{}^{dH} \boldsymbol{M}^d \boldsymbol{q}_0{}^d}{\boldsymbol{q}^d(T)^H \boldsymbol{M}^d \boldsymbol{q}^d(T)} \\ & - \int_0^T \boldsymbol{a}^{dH} (\boldsymbol{B}^d \frac{\partial \boldsymbol{q}^d}{\partial t} + \boldsymbol{A}^d \boldsymbol{q}^d) dt - \boldsymbol{b}^{dH} (\boldsymbol{q}^d(0) - \boldsymbol{q}_0{}^d).\end{aligned} \tag{4.5}$$

The constraints are paired with Lagrange multipliers $\boldsymbol{a}^d$ and $\boldsymbol{b}^d$ which appear as new variables. Equating the derivatives with respect to each of the variables to zero specifies

the optimality conditions:

$$\frac{\partial \mathcal{L}^d}{\partial \boldsymbol{a}^d} = \mathbf{0} \Rightarrow \boldsymbol{B}^d \frac{\partial \boldsymbol{q}^d}{\partial t} + \boldsymbol{A}^d \boldsymbol{q}^d = \mathbf{0}, \tag{4.6a}$$

$$\frac{\partial \mathcal{L}^d}{\partial \boldsymbol{b}^d} = \mathbf{0} \Rightarrow \boldsymbol{q}^d(0) = {\boldsymbol{q}_0}^d, \tag{4.6b}$$

$$\frac{\partial \mathcal{L}^d}{\partial {\boldsymbol{q}_0}^d} = \mathbf{0} \Rightarrow \frac{2}{E^d(T)} {\boldsymbol{q}_0}^{dH} \boldsymbol{M}^d = {\boldsymbol{a}^d(0)}^H \boldsymbol{B}^d, \tag{4.6c}$$

$$\frac{\partial \mathcal{L}^d}{\partial \boldsymbol{q}^d} = \mathbf{0} \Rightarrow \frac{2\ E^d(0)}{E^d(T)^2} \boldsymbol{q}^d(T) \boldsymbol{M}^d = -{\boldsymbol{a}^d(T)}^H \boldsymbol{B}^d, \tag{4.6d}$$

$$\Rightarrow (\frac{\partial \boldsymbol{a}^d}{\partial t})^H \boldsymbol{B}^d + {\boldsymbol{a}^d}^H \boldsymbol{A}^d = \mathbf{0}. \tag{4.6e}$$

(4.6a) is the state equations from (4.1) with initial condition (4.6b). The optimality condition (4.6c) is updating the initial condition for the state equation. (4.6d) represents the adjoint initial condition for the adjoint system (4.6e).

4.3 First Optimized, Then Discretized

In this approach the Lagrange function is set up in the continuous form which reads

$$\begin{aligned}\mathcal{L}(\boldsymbol{q}_1(t), \boldsymbol{q}_2(t), \boldsymbol{q}_0, \boldsymbol{q}_1^a(t), \boldsymbol{q}_2^a(t), \xi, \xi^a) &= J(\boldsymbol{q}(T), \boldsymbol{q}_0) - \\ &- \left[\int_0^T \int_{\Omega_1} (\boldsymbol{q}_1^a, \boldsymbol{B}_1 \frac{\partial \boldsymbol{q}_1}{\partial t} + \boldsymbol{A}_1 \boldsymbol{q}_1) dy dt + \int_0^T \int_{\Omega_2} (\boldsymbol{q}_2^a, \boldsymbol{B}_2 \frac{\partial \boldsymbol{q}_2}{\partial t} + \boldsymbol{A}_2 \boldsymbol{q}_2) dy dt \right] \\ &- \int_0^T (\xi^a, \frac{\partial \xi}{\partial t} + i\alpha U_1 \xi - v_1) dt = 0 \end{aligned} \tag{4.7}$$

with the Lagrange multipliers $\boldsymbol{q}_1^a(t)$, $\boldsymbol{q}_2^a(t)$ and $\xi^a(t)$. This gives after directional differentiation the optimality system. It is not necessary to introduce Langrange multipliers for each initial and boundary condition. The multipliers appearing here also follow the definition of the adjoint operator and therefore they are equivalently called such. The adjoint counterparts of the differential equations and each condition are achieved implicitly in the next section. The continuous cost functional $J(T)$ can be written by means of the $\boldsymbol{M}$-scalar product from section 3.3:

$$J(T) = \frac{E(0)}{E(T)} = \frac{(\boldsymbol{q}_0, \boldsymbol{q}_0)_{\boldsymbol{M}} + |\xi(0)|^2 \frac{Sk^4}{Re^2}}{(\boldsymbol{q}(T), \boldsymbol{q}(T))_{\boldsymbol{M}} + |\xi(T)|^2 \frac{Sk^4}{Re^2}}. \tag{4.8}$$

4.3.1 Adjoint Equations

In order to find the equations for the adjoint variables, denoted by ^{a}, summarized in $\boldsymbol{A}_1^a$, $\boldsymbol{B}_1^a$, $\boldsymbol{A}_2^a$, $\boldsymbol{B}_2^a$ and the adjoint interface and boundary conditions the following equation

should hold:

$$\int_0^T \int_{\Omega_1} (\boldsymbol{q}_1^a, \boldsymbol{B}_1 \frac{\partial \boldsymbol{q}_1}{\partial t} + \boldsymbol{A}_1 \boldsymbol{q}_1) dy dt + \int_0^T \int_{\Omega_2} (\boldsymbol{q}_2^a, \boldsymbol{B}_2 \frac{\partial \boldsymbol{q}_2}{\partial t} + \boldsymbol{A}_2 \boldsymbol{q}_2) dy dt + \int_0^T (\xi^a, \frac{\partial \xi}{\partial t} + i\alpha U_1 \xi - v_1) dt = \int_0^T \int_{\Omega_1} (\boldsymbol{q}_1, \boldsymbol{B}_1^a \frac{\partial \boldsymbol{q}_1^a}{\partial t} + \boldsymbol{A}_1^a \boldsymbol{q}_1^a) dy dt + \int_0^T \int_{\Omega_2} (\boldsymbol{q}_2, \boldsymbol{B}_2^a \frac{\partial \boldsymbol{q}_2^a}{\partial t} + \boldsymbol{A}_2^a \boldsymbol{q}_2^a) dy dt + \sum_{i=0}^{3} T_{1i} + \sum_{i=0}^{10} S_{1i} + \sum_{i=0}^{4} T_{2i} + \sum_{i=0}^{10} S_{2i}. \tag{4.9}$$

Integration by parts of the left hand side in (4.9) up to the point that all derivatives of the direct variables vanish and appear on the adjoint ones instead, makes it possible to factorize the terms with respect to the direct variables such that the left hand side of (4.9) can be written in terms of the right hand side. The boundary terms are collected in the sums (for detailed formulas see Table 4.2). The adjoint equations then follow for Ω_1

$$-\frac{\partial}{\partial t}(D^2 - k^2) v_1^a + \left[2i\alpha U_1' D + i\alpha U_1 (D^2 - k^2) - \frac{1}{Re}(D^2 - k^2)^2 \right] v_1^a + i\beta U_1' \eta_1^a = 0, \tag{4.10a}$$

$$-\frac{\partial}{\partial t}\eta_1^a + \left[i\alpha U_1 - \frac{1}{Re}(D^2 - k^2) \right] \eta_1^a = 0, \tag{4.10b}$$

and for Ω_2

$$-\frac{\partial}{\partial t}(D^2 - k^2) v_2^a + \left[2i\alpha U_2' D + i\alpha U_2 (D^2 - k^2) - \frac{1}{Re}\frac{m}{\gamma}(D^2 - k^2)^2 \right] v_2^a + i\beta U_2' \eta_2^a = 0 \tag{4.11a}$$

$$-\frac{\partial}{\partial t}\eta_2^a + \left[i\alpha U_2 - \frac{1}{Re}\frac{m}{\gamma}(D^2 - k^2) \right] \eta_2^a = 0 \tag{4.11b}$$

respectively. The boundary terms in (4.9) have to vanish and give the adjoint boundary and interface conditions. In order to find them, the direct interface conditions (3.31b), (3.32), (3.33), (3.34), (3.42), (3.43), (3.48) and the boundary conditions (see Figure 3.4) are inserted. This makes it possible to sort the terms again with respect to the direct variable such that the adjoint boundary conditions read

$$v_1^a(0) = 0, \tag{4.12a}$$

$$v_2^a(t \to \infty) = 0, \tag{4.12b}$$

$$v_1^{a\prime}(0) = 0, \tag{4.12c}$$

$$v_2^{a\prime}(t \to \infty) = 0, \tag{4.12d}$$

$$\eta_1^a(0) = 0, \tag{4.12e}$$

$$\eta_2^a(t \to \infty) = 0, \tag{4.12f}$$

and the interface conditions read

$$v_1^a = \frac{1}{\gamma} v_2^a, \tag{4.13a}$$

$$v_1^{a\prime} = \frac{1}{\gamma} v_2^{a\prime}, \tag{4.13b}$$

$$\eta_1^a = \frac{1}{\gamma} \eta_2^a, \tag{4.13c}$$

$$\eta_1^{a\prime} = \frac{m}{\gamma} \eta_2^{a\prime}, \tag{4.13d}$$

$$2k^2 v_1^a - \frac{(3-m)}{\gamma} k^2 v_2^a - v_1^{a\prime\prime} + \frac{m}{\gamma} v_2^{a\prime\prime} = 0, \tag{4.13e}$$

$$\begin{aligned} Re\frac{\partial}{\partial t}(v_1^{a\prime} - v_2^{a\prime}) - (i\alpha U_1 Re + 2k^2) v_1^{a\prime} + v_1^{a\prime\prime\prime} - \frac{m}{\gamma} v_2^{a\prime\prime\prime} \\ + (\frac{(3m-1)}{\gamma} k^2 + i\alpha U_1 Re) v_2^{a\prime} + Re\xi^a = 0, \end{aligned} \tag{4.13f}$$

$$\begin{aligned} \frac{\partial \xi^a}{\partial t} + i\alpha U_1 \xi^a - i\alpha (U_1' - U_2')(i\alpha U_2 (\frac{1}{\gamma} - 1) + \frac{m}{Re\gamma} k^2) v_2^a \\ + i\alpha (U_1'' - m U_2'') \frac{1}{Re\gamma} v_2^{a\prime} - i\alpha (U_1' - U_2') \frac{m}{Re\gamma} v_2^{a\prime\prime} \\ + i\beta (U_1'' - m U_2'') \frac{m}{Re\gamma} \eta_2^{a\prime\prime} - i\beta (U_1' - U_2') \frac{m}{Re\gamma} \eta_2^{a\prime} \\ - (Sk^4 + \frac{k^2}{Fr^2}(1-\gamma)) \frac{1}{\gamma} v_2^a = 0. \end{aligned} \tag{4.13g}$$

Tab. 4.2: Boundary terms appearing after integration by parts of the adjoint equations for both domains Ω_1 and Ω_2

Ω_1	Ω_2
$T_{10} = \left[\int_{\Omega_1} v_1^a D^2 v_1 dy\right]_0^T$	$T_{20} = \left[\int_{\Omega_2} v_2^a D^2 v_2 dy\right]_0^T$
$T_{11} = \left[\int_{\Omega_1} -v_1^a k^2 v_1 dy\right]_0^T$	$T_{21} = \left[\int_{\Omega_2} -v_2^a k^2 v_2 dy\right]_0^T$
$T_{12} = \left[\int_{\Omega_1} \eta_1^a \eta_1 dy\right]_0^T$	$T_{22} = \left[\int_{\Omega_2} \eta_2^a \eta_2 dy\right]_0^T$
$T_{13} = [\xi^a \xi]_0^T$	
	$T_{23} = \left[(1-\frac{1}{\gamma}) v_2^a v_1'\right]_0^T$
	$T_{24} = [-i\alpha(U_1' - U_2') v_2^a \xi]_0^T$
$S_{10} = \left[\int_0^T -\frac{\partial v_1^a}{\partial t} D v_1 dt\right]_{\partial\Omega_1}$	$S_{20} = \left[\int_0^T -\frac{\partial v_2^a}{\partial t} D v_2 dt\right]_{\partial\Omega_2}$
$S_{11} = \left[\int_0^T \frac{\partial D v_1^a}{\partial t} v_1 dt\right]_{\partial\Omega_1}$	$S_{21} = \left[\int_0^T \frac{\partial D v_2^a}{\partial t} v_2 dt\right]_{\partial\Omega_2}$
$S_{12} = \left[\int_0^T v_1^a (i\alpha U_1 + 2\frac{1}{Re} k^2) D v_1 dt\right]_{\partial\Omega_1}$	$S_{22} = \left[\int_0^T v_2^a (i\alpha U_2 + 2\frac{1}{Re}\frac{m}{\gamma} k^2) D v_2 dt\right]_{\partial\Omega_2}$
$S_{13} = \left[\int_0^T -(v_1^a i\alpha U_1' + D v_1^a (i\alpha U_1 + 2\frac{1}{Re} k^2)) v_1 dt\right]_{\partial\Omega_1}$	$S_{23} = \left[\int_0^T -(v_2^a i\alpha U_2' + D v_2^a (i\alpha U_2 + 2\frac{2}{Re}\frac{m}{\gamma} k^2)) v_2 dt\right]_{\partial\Omega_2}$
$S_{14} = \left[\int_0^T -v_1^a \frac{1}{Re} D^3 v_1 dt\right]_{\partial\Omega_1}$	$S_{24} = \left[\int_0^T -v_2^a \frac{2}{Re}\frac{m}{\gamma} D^3 v_2 dt\right]_{\partial\Omega_2}$
$S_{15} = \left[\int_0^T D v_1^a \frac{1}{Re} D^2 v_1 dt\right]_{\partial\Omega_1}$	$S_{25} = \left[\int_0^T D v_2^a \frac{1}{Re}\frac{m}{\gamma} D^2 v_2 dt\right]_{\partial\Omega_2}$
$S_{16} = \left[\int_0^T -D^2 v_1^a \frac{1}{Re} D v_1 dt\right]_{\partial\Omega_1}$	$S_{26} = \left[\int_0^T -D^2 v_2^a \frac{1}{Re}\frac{m}{\gamma} D v_2 dt\right]_{\partial\Omega_2}$
$S_{17} = \left[\int_0^T -D^3 v_1^a \frac{1}{Re} D v_1 dt\right]_{\partial\Omega_1}$	$S_{27} = \left[\int_0^T -D^3 v_2^a \frac{1}{Re}\frac{m}{\gamma} D v_2 dt\right]_{\partial\Omega_2}$
$S_{18} = \left[\int_0^T -\eta_1^a \frac{1}{Re} D \eta_1 dt\right]_{\partial\Omega_1}$	$S_{28} = \left[\int_0^T -\eta_2^a \frac{1}{Re}\frac{m}{\gamma} D \eta_2 dt\right]_{\partial\Omega_2}$
$S_{19} = \left[\int_0^T D\eta_1^a \frac{1}{Re} \eta_1 dt\right]_{\partial\Omega_1}$	$S_{29} = \left[\int_0^T D\eta_2^a \frac{1}{Re}\frac{m}{\gamma} \eta_2 dt\right]_{\partial\Omega_2}$

4.3.2 Optimality Conditions

The directional derivatives of $\mathcal{L}$ with respect to all variables give the optimality system

$$\frac{\partial \mathcal{L}}{\partial \boldsymbol{q}_1^a} = \mathbf{0} \Rightarrow \boldsymbol{B}_1 \frac{\partial \boldsymbol{q}_1}{\partial t} + \boldsymbol{A}_1 \boldsymbol{q}_1 = 0 \tag{4.14a}$$

$$\frac{\partial \mathcal{L}}{\partial \boldsymbol{q}_2^a} = \mathbf{0} \Rightarrow \boldsymbol{B}_2 \frac{\partial \boldsymbol{q}_2}{\partial t} + \boldsymbol{A}_2 \boldsymbol{q}_2 = 0 \tag{4.14b}$$

$$\frac{\partial \mathcal{L}}{\partial \boldsymbol{q}_0} = \mathbf{0} \Rightarrow \frac{2}{E(T)} \boldsymbol{q}_0{}^H \boldsymbol{M} = \boldsymbol{q}^a(0)^H \boldsymbol{B} \tag{4.14c}$$

$$\frac{\partial \mathcal{L}}{\partial \boldsymbol{q}_1} = \mathbf{0} \Rightarrow \frac{2\ E(0)}{E(T)^2} \boldsymbol{q}_1(T) \boldsymbol{M}_1 = -\boldsymbol{q}_1^a(T)^H \boldsymbol{B}_1 \tag{4.14d}$$

$$\Rightarrow \boldsymbol{B}_1^a \frac{\partial \boldsymbol{q}_1^a}{\partial t} + \boldsymbol{A}_1^a \boldsymbol{q}_1^a = 0 \tag{4.14e}$$

$$\frac{\partial \mathcal{L}}{\partial \boldsymbol{q}_2} = \mathbf{0} \Rightarrow \frac{2\ E(0)}{E(T)^2} \boldsymbol{q}_2(T) \boldsymbol{M}_2 = -\boldsymbol{q}_2^a(T)^H \boldsymbol{B}_2 \tag{4.14f}$$

$$\Rightarrow \boldsymbol{B}_2^a \frac{\partial \boldsymbol{q}_2^a}{\partial t} + \boldsymbol{A}_2^a \boldsymbol{q}_2^a = 0 \tag{4.14g}$$

$$\frac{\partial \mathcal{L}}{\partial \xi} = \mathbf{0} \Rightarrow (4.2) \quad \text{change (4.2) to (4,13g)} \tag{4.14h}$$

$$\frac{\partial \mathcal{L}}{\partial \xi^a} = \mathbf{0} \Rightarrow \frac{\partial \xi}{\partial t} + i\alpha U_1 \xi - v_1 = 0 \tag{4.14i}$$

Discretization of (4.14a) - (4.14i) and writing the conditions for both fluids in terms of matrix-vector equations depending on $\boldsymbol{q}^d$, $\boldsymbol{A}^d$, $\boldsymbol{B}^d$, $\boldsymbol{M}$ and $\boldsymbol{q}^{ad}$, $\boldsymbol{A}^{ad}$, $\boldsymbol{B}^{ad}$, $\boldsymbol{M}^{ad}$ respectively similarly to (4.6e), give the optimality system for this approach. It can be written in the same way as for the *first discretized, then optimized* approach, but the coefficients in the discrete matrix are different. Instead of adjoining the matrices from the direct system, the continuous equations and conditions form the adjoint system.

The implementation of the optimality system *first optimized, then discretized* can be understood from the coding excepts in Listing A.2.

Chapter 5

Verification: Nonmodal Growth in Oscillatory Stokes Flows

Biau (2016) examined in his work transient growth of perturbations in an oscillating single-fluid flow using a similar method that has been developed for the present work. For the purpose of verification, the two-fluid code has been simplified by excluding the surface and assuming the upper fluid to vanish. Those results have been compared with the one published in the article mentioned above. In the following governing equations, the optimality system and discretization will be presented shortly as this setting depicts a simplification of our two-fluid case, explicitly described in chapter 3 and chapter 4.

5.1 Governing Equations and Boundary Conditions

For a single fluid over an oscillating plate the governing equations are the Navier-Stokes-equations as introduced and simplified in section 3.2. Proceeding accordingly for one fluid only ($\rho_1 = \rho_2$), we arrive at the following system which governs the base flow

$$\frac{\partial U}{\partial t} = \frac{1}{Re}\frac{\partial^2 U}{\partial y^2}, \tag{5.1a}$$

$$\frac{\partial p}{\partial y} = -\frac{1}{Fr^2} \tag{5.1b}$$

with the oscillating and zero boundary conditions

$$U(y = 0, t) = \cos(\omega t), \tag{5.2a}$$

$$U(y \to \infty, t) = 0. \tag{5.2b}$$

An analytical solution for this boundary value problem

$$U(y,t) = e^{-c_s y}\ \cos(\omega t - c_s y) \quad \text{with } c_s = \sqrt{\frac{1}{2} Re\omega}, \tag{5.3}$$

which can be found by using complex numbers and separation of variables as presented in subsection 3.2.2. Figure 5.1 shows the velocity profiles of an oscillating base flow at different instants in time.

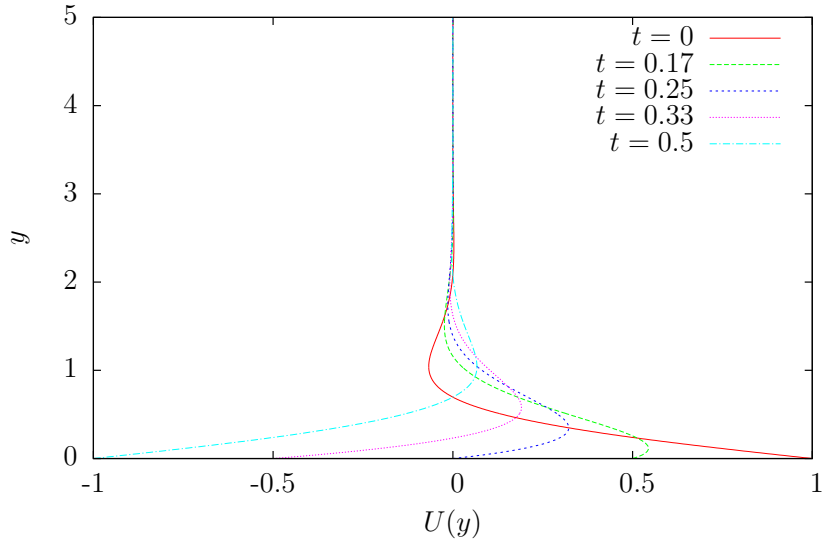

Fig. 5.1: Velocity profiles of an oscillating base flow at different instants in time

Again proceeding as shown in the case for two fluids, the partial differential equations for the perturbations written in terms of v and η are

$$\left(D^2 - k^2\right)\frac{\partial v}{\partial t} + \underbrace{\left[i\alpha\left(D^2 - k^2\right)U - i\alpha U'' - \frac{1}{Re}\left(D^2 - k^2\right)^2\right]}_{=:\,A_{11}} v = 0, \tag{5.4a}$$

$$\frac{\partial \eta}{\partial t} + \underbrace{\left[i\alpha U - \frac{1}{Re}\left(D^2 - k^2\right)\right]}_{=:\,A_{22}}\eta - i\beta U' v = 0. \tag{5.4b}$$

We can write this as a matrix vector equation

$$\underbrace{\begin{bmatrix} D^2 - k^2 & 0 \\ 0 & 1 \end{bmatrix}}_{=:\,\mathbf{B}} \frac{\partial}{\partial t}\begin{bmatrix} v \\ \eta \end{bmatrix} + \underbrace{\begin{bmatrix} A_{11} & 0 \\ i\beta U' & A_{22} \end{bmatrix}}_{=:\,\mathbf{A}} \begin{bmatrix} v \\ \eta \end{bmatrix} = 0 \tag{5.5}$$

ending up with the following initial value problem

$$\begin{aligned} \mathbf{B}\frac{\partial \mathbf{q}}{\partial t} + \mathbf{A}\mathbf{q} &= \mathbf{0}, \\ \mathbf{q}(t=0) &= \mathbf{q_0}. \end{aligned} \tag{5.6}$$

This initial value problem is subject to minimizing the cost functional introduced in the beginning of chapter 4. By means of the Lagrange functional the optimality system in the continuous form can be specified.

5.2 ω-independent Scaling

It is possible to write the analytical solution of the base flow independent from ω, which also reduces the number of parameters. This is done by scaling the Navier-Stokes equations

as proposed by Biau (2016) . The Reynolds number is then $Re_B = u_0^* \sqrt{\frac{T^*}{\nu^*}}$ which concludes from the fact that the time is made dimensionless with the periode P: $t^* = P^* t$. The conversion between the dimensionless variables from each scaling is the following, where $_B$ denotes the quantities scaled from Biau (2016):

$$t = t_B \frac{2\pi}{\omega} \tag{5.7}$$

$$Re = Re_B^2 \frac{\omega}{2\pi} \tag{5.8}$$

$$\alpha = \alpha_B \frac{2\pi}{\omega}. \tag{5.9}$$

This scaling is used in the numerical experiments in order to compare the here presented results with the ones from Biau (2016). The times t_{in} and t_{fin} are given as ratio of a full period P.

5.3 Discretization

For the spatial discretization shown in Figure 5.2 we chose an equally spaced grid with the step size $\delta y = \frac{y_{max}}{n_y}$ where y_{max} denotes the fluid height over the plate for which we solve (5.6) and n_y the number of points within. To approximate in the v equation the fourth derivative at a certain point we need two points above and below, a five point stencil. At the borders we imply the boundary conditions also shown in Figure 5.2.

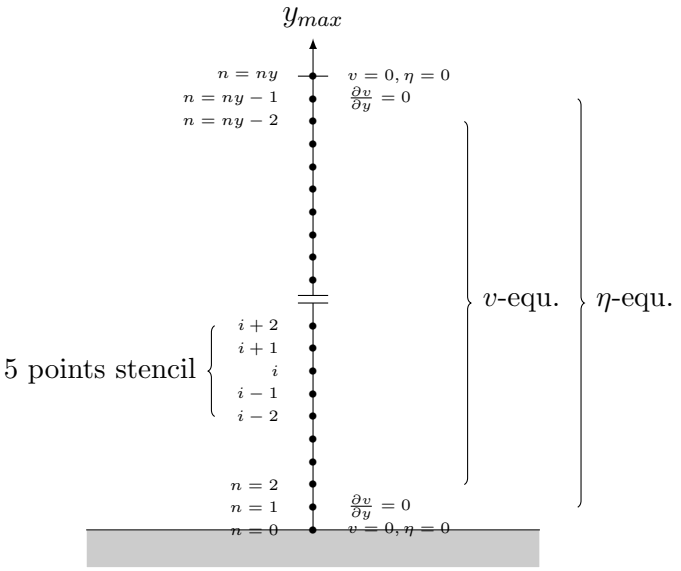

Fig. 5.2: Spatial discretisation in the case of a single fluid

The coefficients for the discrete derivatives are shown in Table 4.1 of section 4.1.

For the discretization in time we chose the three-step Adams-Bashforth method backward in time such that

$$\mathbf{B}^d \frac{d\mathbf{u}^d}{dt} = \frac{1}{\Delta t}(\frac{3}{2}\,\mathbf{B}^d{}_n\,\boldsymbol{u}^d{}_n - 2\,\mathbf{B}^d{}_{n-1}\,\boldsymbol{u}^d{}_{n-1} + \frac{1}{2}\,\mathbf{B}^d{}_{n-2}\,\boldsymbol{u}^d{}_{n-2}).$$

Applied to (5.6) the discrete equation reads

$$\begin{aligned}&\frac{1}{\Delta t}(\frac{3}{2}\,\mathbf{B}^d{}_n\,\boldsymbol{u}^d{}_n - 2\,\mathbf{B}^d{}_{n-1}\,\boldsymbol{u}^d{}_{n-1} + \frac{1}{2}\,\mathbf{B}^d{}_{n-2}\,\boldsymbol{u}^d{}_{n-2}) + \mathbf{A}^d_n\,\mathbf{q}^d{}_n = \mathbf{0}\\ &\Rightarrow (\frac{3}{2\Delta t}\mathbf{B}^d{}_n + \mathbf{A}^d_n)\,\mathbf{q}^d{}_n = \frac{2}{\Delta t}\,\mathbf{B}^d{}_{n-1}\,\mathbf{q}^d{}_{n-1} - \frac{1}{2\Delta t}\,\mathbf{B}^d{}_{n-2}\,\mathbf{q}^d{}_{n-2}.\end{aligned}$$

But because $\mathbf{B}^d$ doesn't depend on time, $\mathbf{B}^d_{n-1} = \mathbf{B}^d_{n-2} =: \mathbf{D}^d$ and with $\mathbf{C}^d_n := (\frac{3}{2\Delta t}\mathbf{B}^d_n + \mathbf{A}^d_n)$ we have to solve the following system as constraint condition

$$\mathbf{C}^d_n\,\mathbf{q}^d_n = \mathbf{D}^d(\frac{2}{\Delta t}\,\mathbf{q}^d_{n-1} - \frac{1}{2\Delta t}\,\mathbf{q}^d_{n-2}).$$

5.4 Optimization Problem and Optimality Conditions

In order to solve our discrete optimization problem

$$\min_{\boldsymbol{q}_0 \neq 0} J^d(\boldsymbol{q}^d_0) \quad \text{s. t.} \quad \mathbf{B}^d\frac{\partial \mathbf{q}^d}{\partial t} + \mathbf{A}^d\boldsymbol{q}^d = \mathbf{0} \text{ in } \Omega^d, 0 < t \leq T \qquad \mathbf{q}^d(0) = \mathbf{q}^d_0 \text{ in } \Omega, t = 0, \tag{5.10}$$

we have to specify our cost functional $J(\mathbf{q}_0)$:

$$J(\mathbf{q}^d_0) = \frac{E^d(\mathbf{q}^d(t=0))}{E^d(\mathbf{q}^d(t=T))} \quad \text{with} \quad E^d(\mathbf{q}^d(t)) := \frac{1}{2k^2}\int_0^{y_{max}} |Dv^d|^2 + k^2|v^d|^2 + |\eta^d|^2 dy. \tag{5.11}$$

As shown in section 3.3 we can write $E^d(\mathbf{q}^d(t))$ with the matrix $\mathbf{M}^d$. Approximating the continuous integral as a discrete sum $E^d(\mathbf{q}^d(t)) \approx \frac{1}{2k^2}\mathbf{q}^d(t)^H\mathbf{M}^d\boldsymbol{q}^d(t)\delta y$, the variations of the discrete Lagrange function

$$\begin{aligned}\mathcal{L}^d(\mathbf{q}^d(t), \mathbf{q}^d_0, \mathbf{a}^d, \mathbf{b}^d) :=& \frac{\mathbf{q}_0^{dH}\mathbf{M}^d\boldsymbol{q}^d_0}{\mathbf{q}^d(T)^H\mathbf{M}^d\boldsymbol{q}^d(T)}\\ &- \int_0^T \mathbf{a}^{dH}(\mathbf{B}^d\frac{\partial \mathbf{q}^d}{\partial t} + \mathbf{A}^d\boldsymbol{q}^d)dt - \mathbf{b}^{dH}(\mathbf{q}^d(0) - \mathbf{q}^d_0),\end{aligned} \tag{5.12}$$

where $\mathbf{a}^d$ and $\mathbf{b}^d$ denote Lagrange multipliers, can be used deducing the optimality conditions (shown in subsection 4.2.2). The discrete optimality systems then reads the following

$$\mathbf{B}^d \frac{\partial \mathbf{q}^d}{\partial t} + \mathbf{A}^d \boldsymbol{q}^d = \mathbf{0} \tag{5.13a}$$

$$\mathbf{q}^d(0) = \mathbf{q}_0^d \tag{5.13b}$$

$$\mathbf{B}^{dH}\mathbf{a}^d(0) = \frac{2}{\mathbf{q}^d(T)^H \mathbf{M}^d \boldsymbol{q}^d(T)} \mathbf{M}^{dH}\mathbf{q}^d(0) = \frac{2}{E^d(T)}\mathbf{M}^{dH}\mathbf{q}^d(0) \tag{5.13c}$$

$$\mathbf{B}^{dH}\frac{\partial \mathbf{a}^d}{\partial t} - \mathbf{A}^{dH}\mathbf{a}^d = \mathbf{0} \tag{5.13d}$$

$$\mathbf{a}^d(T)^H \mathbf{B}^d = -\frac{2\mathbf{q}^d(0)^H \mathbf{M}^d \boldsymbol{q}^d(0)}{(\mathbf{q}^d(T)^H \mathbf{M}^d \boldsymbol{q}^d(T))^2}\mathbf{q}^d(T)^H\mathbf{M}^d = -\frac{2E^d(0)}{E^d(T)^2}\mathbf{q}^d(T)^H\mathbf{M}^d. \tag{5.13e}$$

Comparing $\mathbf{M}^d$ with $\mathbf{B}^d$ shows that we can find a matrix $\mathbf{K}^d$ such that

$$\mathbf{M}^d = \mathbf{K}^d\mathbf{B}^d, \quad \text{with } \mathbf{K}^d = \begin{bmatrix} 1 & 0 & 0 & 0 & 0 & \dots & \dots & \dots & 0 \\ 0 & 1 & 0 & 0 & 0 & \dots & \dots & \dots & 0 \\ 0 & 0 & -1 & 0 & 0 & \dots & \dots & \dots & 0 \\ 0 & 0 & 0 & 1 & 0 & \dots & \dots & \dots & 0 \\ \dots & \dots & \dots & \dots & \ddots & \dots & \dots & \dots & \dots \\ 0 & \dots & \dots & \dots & 0 & -1 & 0 & 0 & 0 \\ 0 & \dots & \dots & \dots & 0 & 0 & 1 & 0 & 0 \\ 0 & \dots & \dots & \dots & 0 & 0 & 0 & 1 & 0 \\ 0 & \dots & \dots & \dots & 0 & 0 & 0 & 0 & 1 \end{bmatrix}. \tag{5.14}$$

The optimality conditions (5.13c) and (5.13e) then simplify to

$$\begin{aligned} & \mathbf{B}^{dH}\mathbf{a}^d(0) = \frac{2}{E^d(T)}\mathbf{B}^{dH}\mathbf{K}^{dH}\mathbf{q}^d(0) \\ \Rightarrow \quad & \mathbf{q}^d(0) = \frac{E^d(T)}{2}(\mathbf{K}^{dH})^{-1}\mathbf{a}^d(0) \qquad (5.15) \\ & \mathbf{a}^d(t)^H\mathbf{B}^d = -\frac{2E^d(0)}{E^d(T)^2}\mathbf{q}^d(t)^H\mathbf{K}^d\boldsymbol{B}^d \\ \Rightarrow \quad & \mathbf{a}^d(t)^H = -\frac{2E^d(0)}{E^d(T)^2}\mathbf{q}^d(t)^H\mathbf{K}^d. \qquad (5.16) \end{aligned}$$

The schematic optimization algorithm developed in order to solve the discrete version of (5.10) can be understood from algorithm 1.

Data: $\mathtt{q_0}, \mathtt{t_{in}}, \mathtt{dt}, \mathtt{dy}, \mathtt{T}, \mathtt{tol}$
Result: $\mathtt{q}$
initialization;
while $\mathtt{err} > \mathtt{tol}$ **do**
  for $\mathtt{n} = 0$ **to** $\mathtt{nt}$ **do**
    $\mathtt{C}^{\mathtt{n}}\,\mathtt{q}^{\mathtt{n}} = \mathtt{D}(\frac{2}{\Delta \mathtt{t}}\,\mathtt{q}^{\mathtt{n}-1} - \frac{1}{2\Delta \mathtt{t}}\,\mathtt{q}^{\mathtt{n}-2})$;
    with initial condition: $\mathtt{q}(0) = \frac{\mathtt{E}(\mathtt{T})}{2}(\mathtt{K}^{\mathtt{H}})^{-1}\mathbf{a}(0)$
  end
  for $\mathtt{n} = \mathtt{nt}$ **to** 0 **do**
    $\mathtt{C}^{\mathtt{nH}}\,\mathtt{a}^{\mathtt{n}} = \mathtt{D}^{\mathtt{H}}(\frac{2}{\Delta \mathtt{t}}\,\mathtt{a}^{\mathtt{n}-1} - \frac{1}{2\Delta \mathtt{t}}\,\mathtt{a}^{\mathtt{n}-2})$;
    with initial condition: $\mathtt{a}(\mathtt{T}) = -\frac{2\mathtt{E}(0)}{\mathtt{E}(\mathtt{T})^2}\mathtt{K}^{\mathtt{H}}\mathtt{q}(\mathtt{T})$
  end
  derive $\mathtt{err}$;
end

Algorithm 1: Optimization loop for a single fluid; integrating the direct forward and the adjoint system backward in time

5.5 Numerical Results

For the case presented in this chapter a full parameter study has not been done in order to find the optimal values because the aim of this thesis was to find the optimal values in a two-fluid flow. The purpose of this chapter is to make sure that the methods applied make sense in a case where a work exists and the results can be compared with. Numerical experiments showed that the optimal values published in (Biau, 2016, p. 7) are also optimal according to the here presented setting, see Figure 5.3 and Figure 5.4, which show a variation of α_B, β and t_{in} as summarized in Table 5.1.

Tab. 5.1: Variation of the optimal values publishes in (Biau, 2016, p. 7).

	var_-	Biau	var_+
α_B	0.667	0.767	0.867
β	-	0	0.1
t_{in}	0.0623	0.0723	0.0823

The behavior of the numerical results for different values of dt and n_y can be seen in Figure 5.5. The variations of dt and n_y has a big influence on the results, as can be seen on the shape of the curve which has not converged with $n_y = 6000$. This can be traced back to the shape of the velocity profile, which shows a rapid change close to the wall. In order to have a sufficient resolution, dt and n_y have to be chosen carefully. In Figure 5.6 it is shown that we could also reproduce the energy curve with its characteristic shape Biau published in his paper up to a high level of accuracy. The small deviation one can detect after $t = 0.5$ might has its origin in the value of n_y. But as a characteristic reproduction of the energy curve was possible, there was no need to increase the spatial steps even more in order to meet the exact values.
Figure 5.7 shows on the top the contours of the spanwise vorticity of the perturbations

$\nu = \frac{\partial v}{\partial x} - \frac{\partial u}{\partial y}$ at $t_{in} = 0.0723$ and at $t_{fin} = 0.4$. The lower two pictures show the v component of the perturbations in order to visualize their evolution. The results are indeed very similar to the once in (Biau, 2016, p. 7).
All together the here presented results confirm the procedure chosen for the confrontation of the two-fluid case.

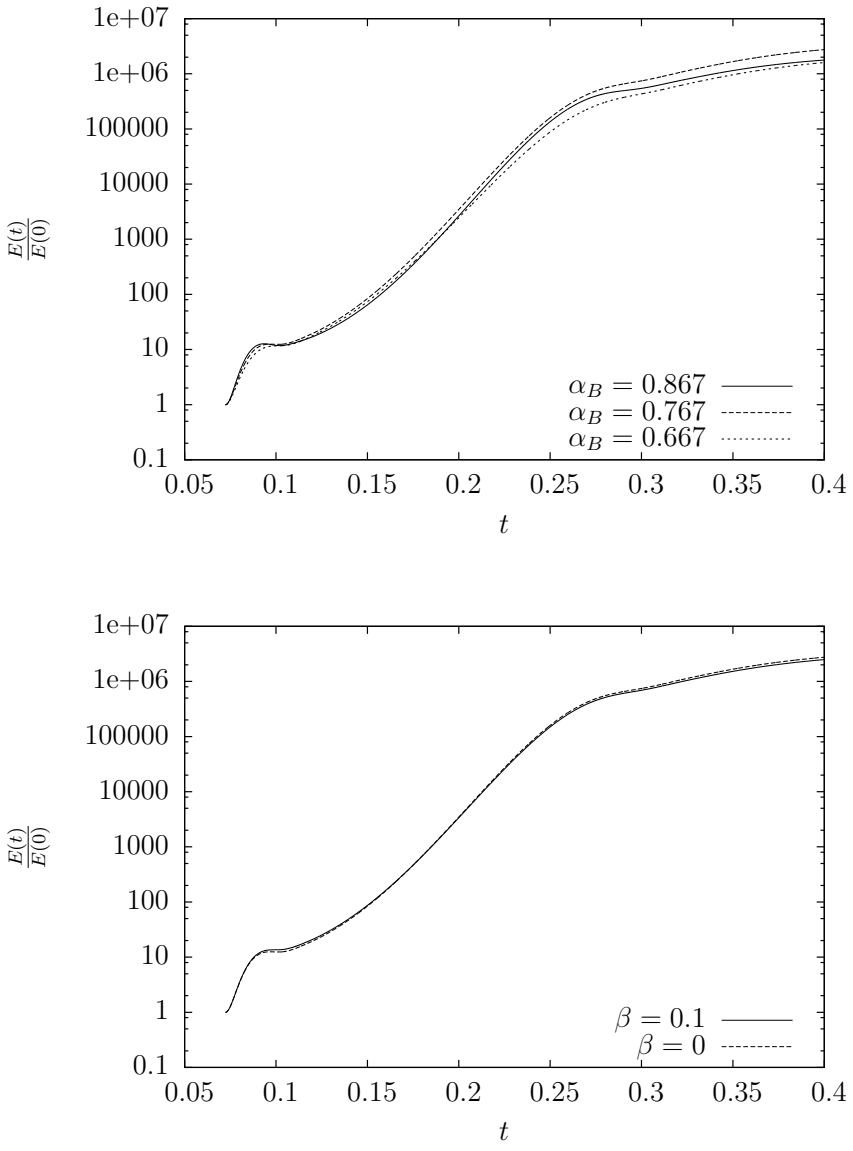

Fig. 5.3: Evolution of normalized energy $\frac{E(t)}{E(0)}$ for varying α_B (top) and β (bottom) and $Re_B = 1000$, $t_{fin} = 0.4$, $dt = 0.0001$, $y_{max} = 15$, $n_y = 3000$

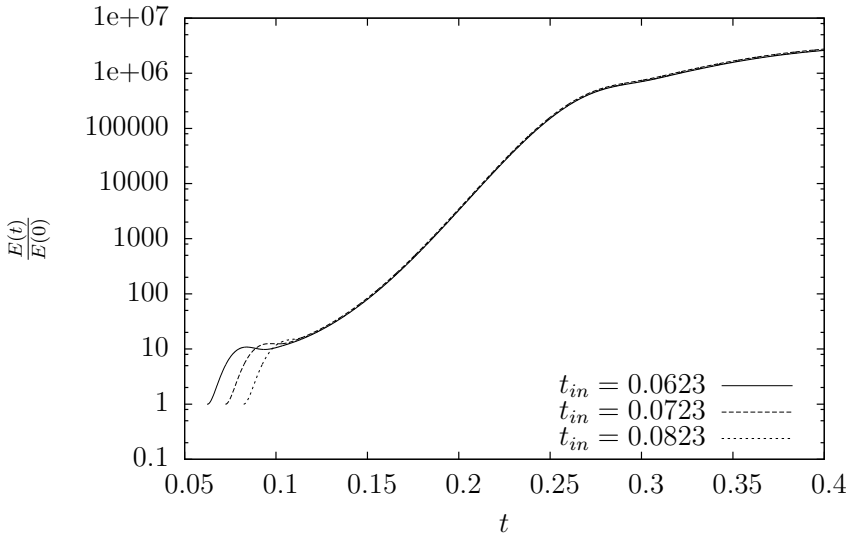

Fig. 5.4: Evolution of normalized energy $\frac{E(t)}{E(0)}$ for varying t_{in} and $Re_B = 1000$, $t_{fin} = 0.4$, $dt = 0.0001$, $y_{max} = 15$, $n_y = 3000$

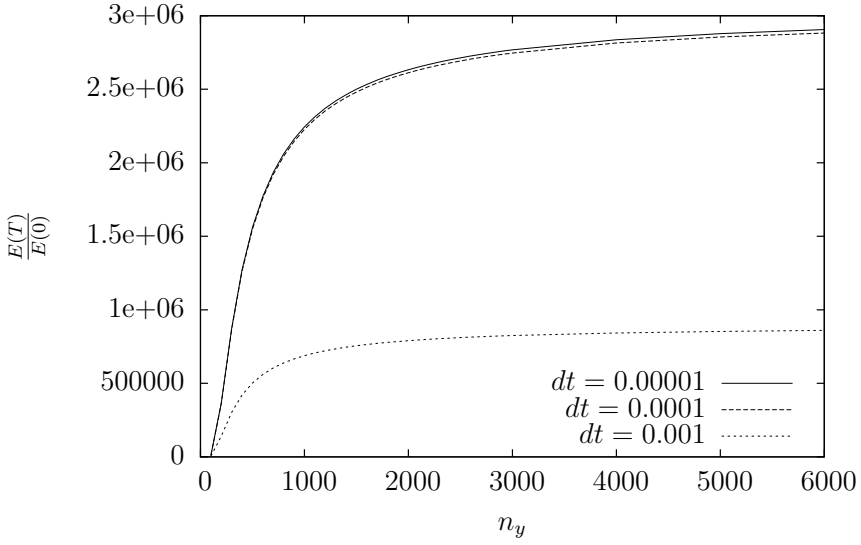

Fig. 5.5: Evolution of maximal normalized energy $\frac{E(T)}{E(0)}$ for different timesteps dt and discrete resolution n_y and $Re_B = 1000$, $\alpha_B = 0.767$, $\beta = 0$, $t_{in} = 0.0723$, $t_{fin} = 0.4$, $y_{max} = 15$

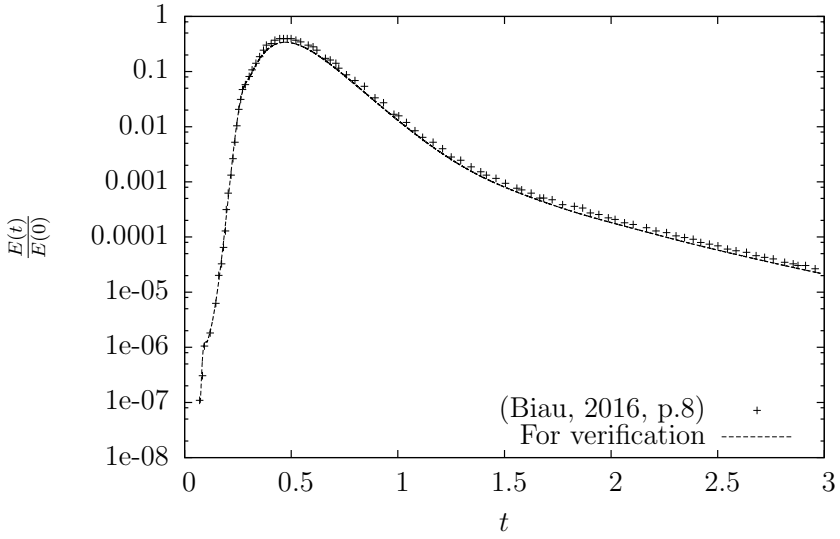

Fig. 5.6: Evolution of normalized energy $\frac{E(t)}{E(0)}$ in comparison with results by Biau (2016) and $R_B = 1000$, $\alpha_B = 0.767$, $\beta = 0$, $t_{in} = 0.0723$, $t_{fin} = 3.0$, $dt = 0.0001$, $y_{max} = 15$, $n_y = 3000$

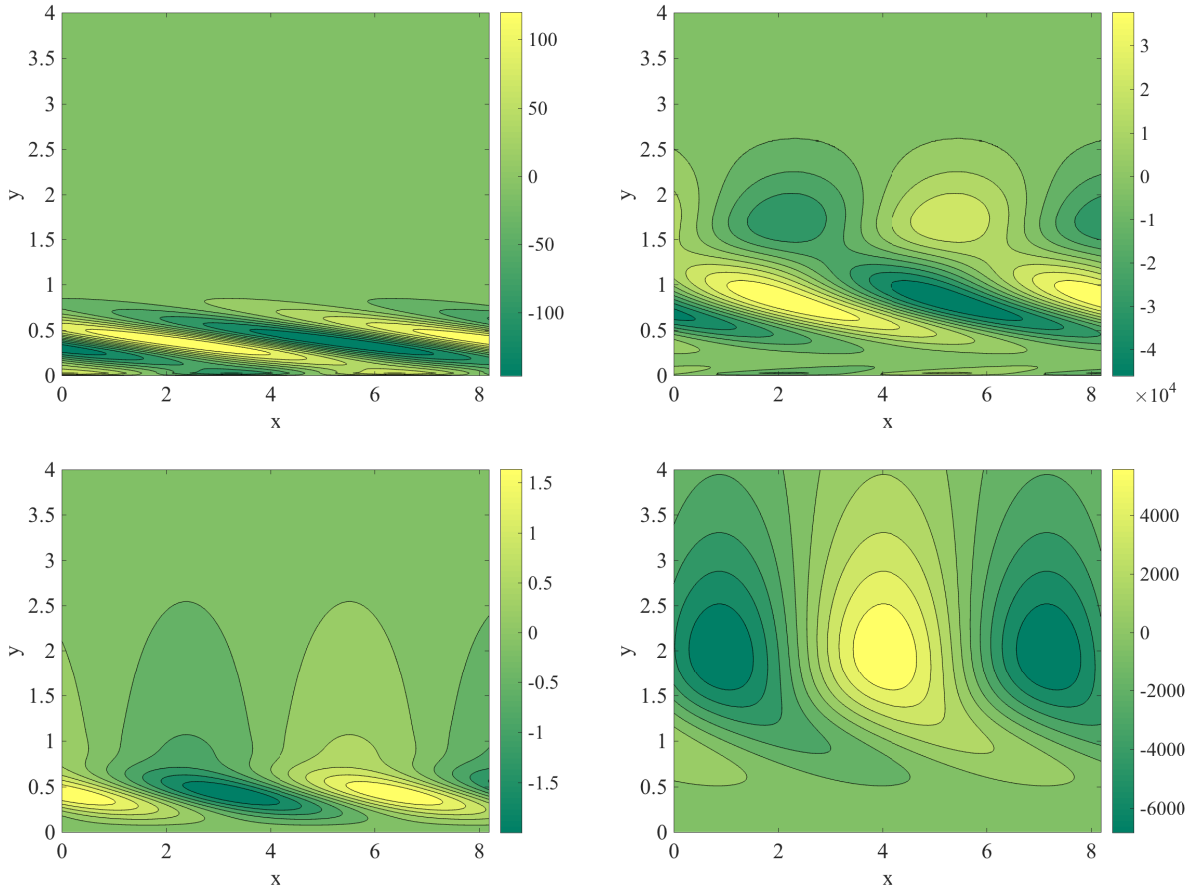

Fig. 5.7: Contours of the spanwise vorticity $\nu = \frac{\partial v}{\partial x} - \frac{\partial u}{\partial y}$ (top) and v (bottom) of the perturbations at $t_{in} = 0.0723$ (left) and $t_{fin} = 0.4$ (right), normalized with respect to $|v(t = 0)|$

Chapter 6

Results

This chapter is divided in two parts where section 6.1 contains a study of the parameters and section 6.2 deals with the individual application of the eye after vitrectomy. The results here presented are produced by applying the *first optimized, then discretized* approach (for some relevant excerpts see Appendix A). A code in which the system has discretized first and then optimized was tested as well but led to numerical problems, most likely due to the unfavorable condition of the discrete matrices, so that the results were not exploitable. In order to evaluate the quality of the findings on basis of a reference, the case from Biau (2016) is again the starting point from which the parameters, namely viscosity ratio m and surface tension S, vary such that a two-fluid case is obtained with similar flow characteristics.
The objective of the experiments are to find the optimal spanwise and streamwise wavenumber α and β as well as the optimal initial and final time t_{in} and t_{fin} for different values of the viscosity ratio m. For each different case depending of the flow characteristics and the densities of the two fluids the optimal values change. The wavenumbers govern the shape of the perturbation $u(y,t)e^{i(\alpha x+\beta z)}$ and t_{in} and t_{fin} the shape of the base flow. In order to find the worst case scenario the normalized energy at some instant of time T $\frac{E(T)}{E(0)}$ functions as a measure of the amplifications.

6.1 Parameter Study

This study is done for the case $Re_B = 1000$, $Fr = 20$, $\gamma = 1$, $\omega = 0.008$ and $y_{max} = 15$. The numerical parameters are $n_{y1} = 200$ and $dt = 0.5$. The Reynolds number and α are denoted with $_B$ which refers to the scaling of Biau (2016) for which a conversion can be done by (5.8) and (5.9) in section 5.2. The times t_{in} and t_{fin} are understood in terms of the fraction of a full period $P = \frac{2\pi}{\omega}$.

6.1.1 Influence of Viscosity Ratio m

In order to understand the influence of m on the optimal values of α and β different cases are presented in Figure 6.1 which show the energy at final time $t = T$ normalized with the initial energy at $t = 0$ for different values of m in the α-β plane. In the top left picture the single fluid case with vanishing surface tension and no viscosity difference is shown followed by the case of two identical fluids but surface tension (top right). Below there are one case with $m = 5$ and one case with $m = 10$. The contour lines are drawn at the same levels in each picture.

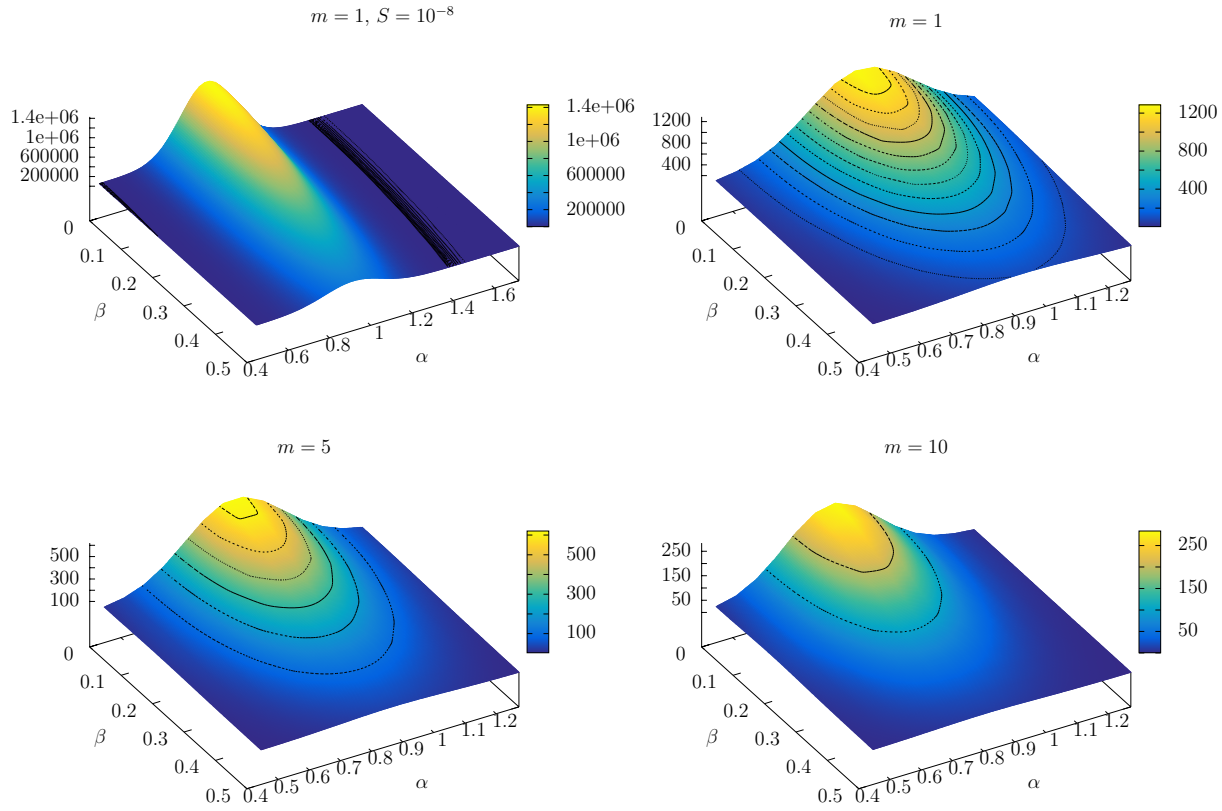

Fig. 6.1: Maximal normalized energy $\frac{E(T)}{E(0)}$ showed as surface parametrized with α and β for different values of m and $t_{in} = 0.0723$, $t_{fin} = 0.4$, $Re_B = 1000$, $dt = 0.5$, $y_{max} = 15$, $n_{y1} = 200$, $Fr = 20$, $\gamma = 1$, $\omega = 0.008$. In all subfigures $S = 0.1$ except for the upper left one where $S = 10^{-8}$ (single fluid approximation)

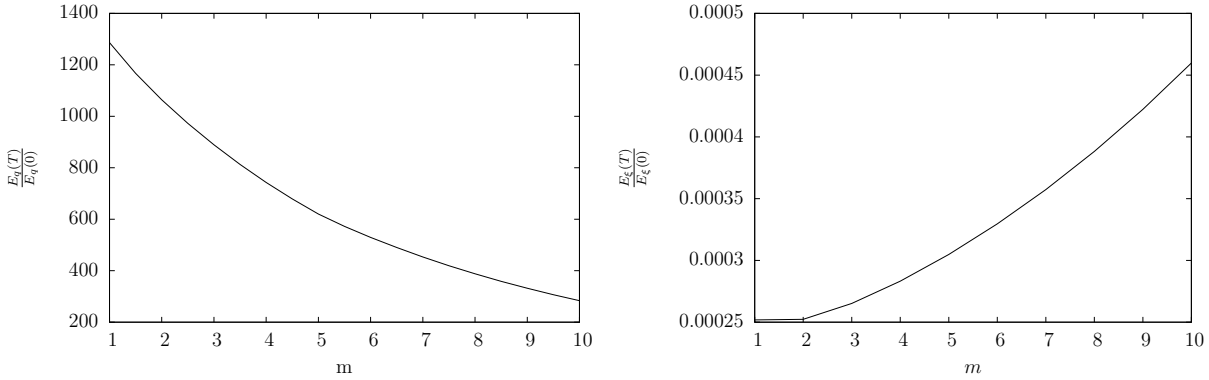

Fig. 6.2: Maximal normalized flow $\frac{E_q(T)}{E_q(0)}$ (left) and interface energy $\frac{E_\xi(T)}{E_\xi(0)}$ (right) for varying m, optimal α and β and $t_{in} = 0.0723$, $t_{fin} = 0.4$, $Re_B = 1000$, $dt = 0.5$, $y_{max} = 15$, $n_{y1} = 200$, $Fr = 20$, $\gamma = 1$, $\omega = 0.008$, $S = 0.1$

It can be understood that the maximal gain $\frac{E(T)}{E(0)}$ decays with growing m. This fact becomes even more obvious from the curve of the maximal flow energy $\frac{E_q(T)}{E_q(0)}$ in Figure 6.2 on the left. On the right in the aforementioned figure the maximal interface energy $\frac{E_\xi(T)}{E_\xi(0)}$ as a function of m is shown. The energy of the interface is growing with m but as its contribution to the total gain is vanishing, it does not come into account for the here chosen range. It can be followed that m has a damping influence on the maximal gain. The optimal β is in all cases 0 and the optimal α is not changing much between 0.7 and 0.65 due to the step size in the α-β resolution and it is most likely that the change is even smaller with higher resolution.
The evolution of the perturbations can be understood from Figure 6.3 and Figure 6.4.

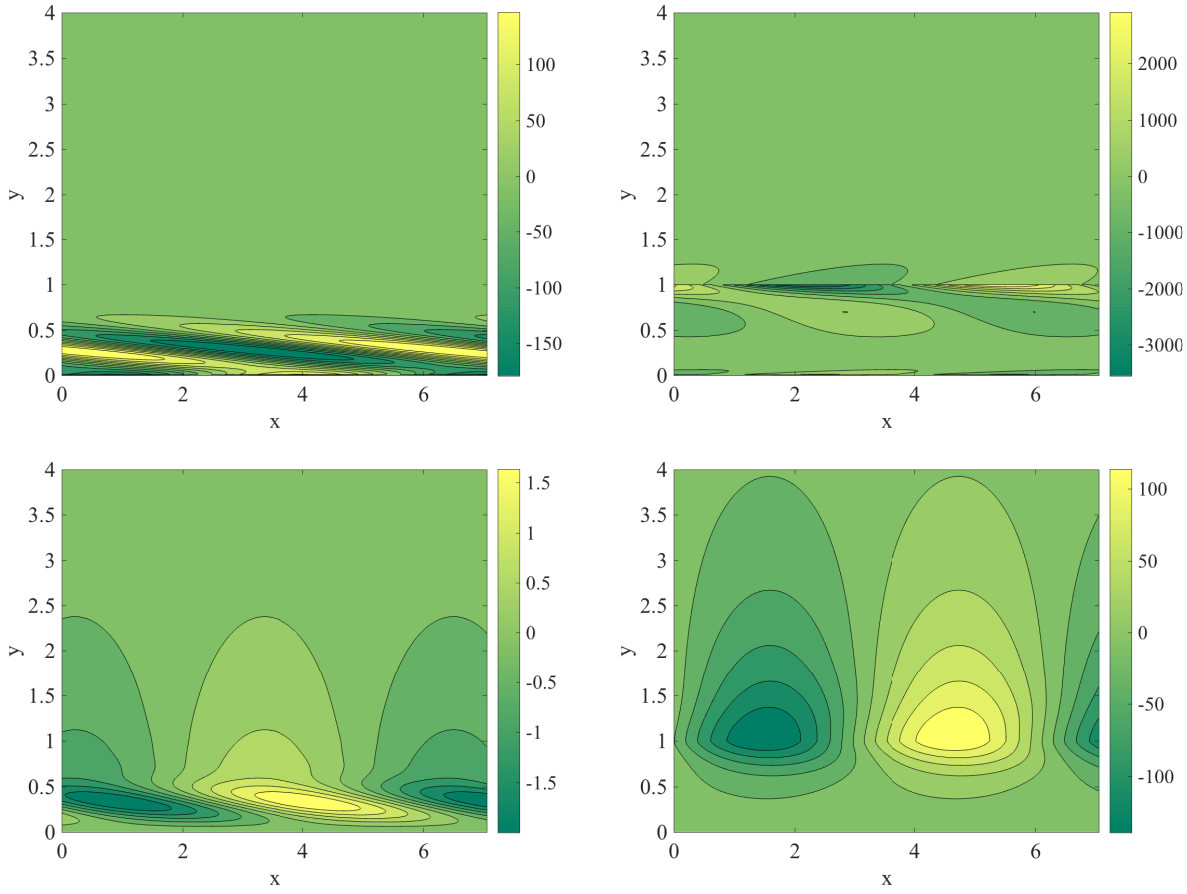

Fig. 6.3: Contours of the spanwise vorticity $\nu = \frac{\partial v}{\partial x} - \frac{\partial u}{\partial y}$ (top) and v (bottom) of the perturbations at $t_{in} = 0.0723$ (left) and $t_{fin} = 0.4$ (right), normalized with respect to $|v(t = 0)|$; $m = 5$, $S = 0.1$, $\alpha_B = 0.7$, $\beta = 0$, $Re_B = 1000$, $dt = 0.5$, $y_{max} = 15$, $n_{y1} = 200$, $Fr = 20$, $\gamma = 1$, $\omega = 0.008$

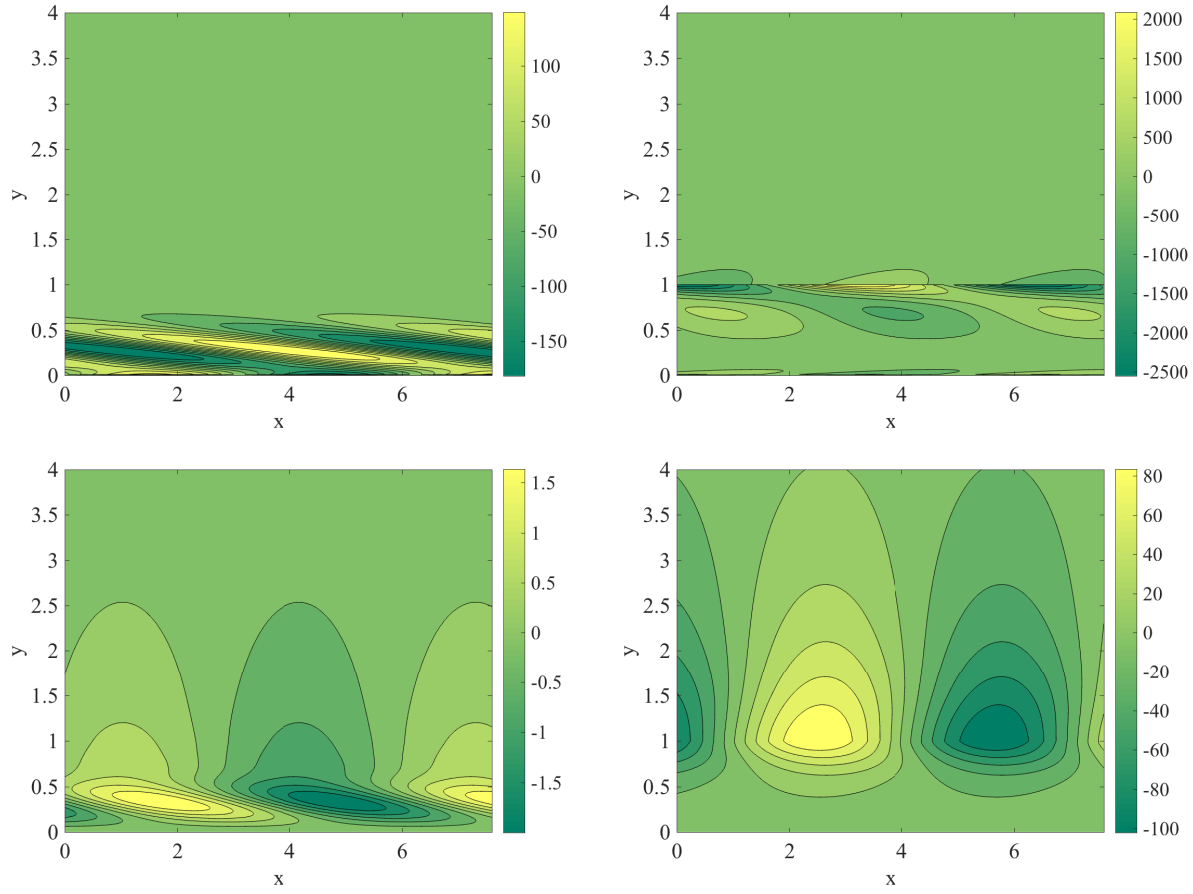

Fig. 6.4: Contours of the spanwise vorticity $\nu = \frac{\partial v}{\partial x} - \frac{\partial u}{\partial y}$ (top) and v (bottom) of the perturbations at $t_{in} = 0.0723$ (left) and $t_{fin} = 0.4$ (right), normalized with respect to $|v(t = 0)|$; $m = 10$, $S = 0.1$, $\alpha_B = 0.65$, $\beta = 0$, $Re_B = 1000$, $dt = 0.5$, $y_{max} = 15$, $n_{y1} = 200$, $Fr = 20$, $\gamma = 1$, $\omega = 0.008$

In each contour-figures the upper row shows the span wise vorticity $\nu = \frac{\partial v}{\partial x} - \frac{\partial u}{\partial y}$ and the lower row the velocity v of the optimal perturbations, on the left at initial time t_{in} and on the right side at final time t_{fin}. The left pictures look very much alike which means that the initial condition in the last optimization loop was in both cases similar. The pictures on the right show a different range of magnitude. The qualitative behavior is very similar. The influence of the spanwise wavenumber β is not apparent. In comparison to Figure 5.7 from section 5.5 the interface at $y = 1$ becomes visible where the velocity v shows kinks. The spanwise vorticity shows extreme values and its shape is significantly flatten.

6.1.2 Influence of t_{in} and t_{fin}

In this subsection the viscosity ratio is fixed to $m = 5$. The time ranges governed by t_{in} and t_{fin} are varied such that nine cases arise. An overview over these can be found in Figure 6.6. The values were chosen by varying the optimal times from the single fluid case with $t_{in} = 0.0723$ and $t_{fin} = 0.4$ (plot in the middle) slightly. In order to capture the maximum of the normalized energy in the α-β plane, the ranges change from case

to case. Here two dimensional plots of the maximal gain in the α-β plane are shown. The contour lines are drawn at the same levels in every plot such that more level curves indicate a higher level of energy at the maximum. Three pictures per row show cases with varying t_{in} and fixed t_{fin}. Read from top to bottom three pictures per column show cases with varying t_{fin} and fixed t_{in}. The top three pictures of Figure 6.6 illustrate cases with $t_{fin} = 0.2$. The one in the middle presents the case with maximal gain out of all nine. The row below has a fixed initial time of $t_{in} = 0.4$ and the one on the bottom $t_{in} = 0.6$. All together, the runs with lowest energy magnitude are the ones with $t_{in} = 0.6$ compared to all others. The first column contains the cases with the lowest energy compared to the others in the row respectively.

The optimal value for the spanwise wavenumber β is 0. The optimal value for α changes with initial and final time. It can be observed that with fixed initial time the optimal α decays with later final time. In case of a fixed final time, optimal α grows with later initial time for cases $t_{fin} = 0.2$, decays for cases with $t_{fin} = 0.6$ and has a maximum at $t_{in} = 0.0723$ for $t_{fin} = 0.4$. This behavior can be seen from plotting the optimal α values in the t_{in}-t_{fin}-plane, see Figure 6.5 on the right. On the left in the figure aforementioned the maximal normalized energy at optimal α respectively shows a clear maximum around $t_{in} = 0.072$ and $t_{fin} = 0.2$.
Fixing the wave numbers by the optimal values from the case with the maximum gain $\alpha_B = 0.87$ and $\beta = 0$, (of Figure 6.6) and searching again in the time-plane refines an optimal time span with $t_{in} = 0.079$ and $t_{fin} = 0.23$, as Figure 6.7 exhibits.

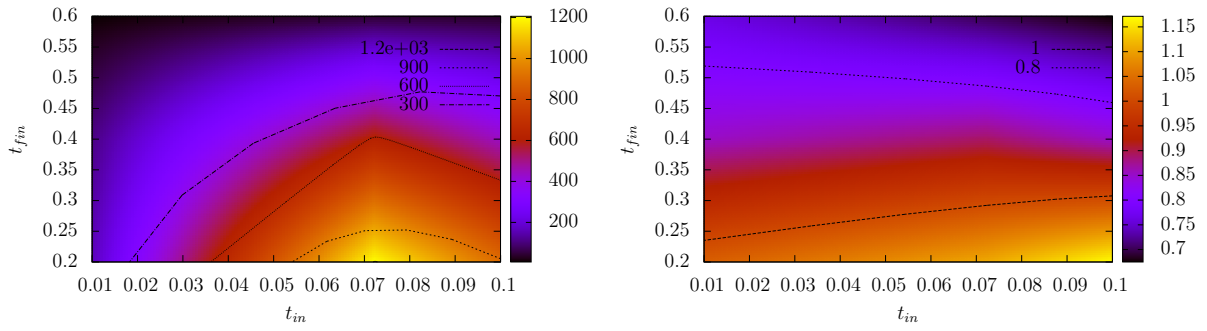

Fig. 6.5: Maximal normalized energy $\frac{E(T)}{E(0)}$ (left) at optimal α respectively; optimal α (right) in the t_{in}-t_{fin} plane with $m = 5$, $S = 0.1$ $Re_B = 1000$, $dt = 0.5$, $y_{max} = 15$, $n_{y1} = 200$, $Fr = 20$, $\gamma = 1$, $\omega = 0.008$

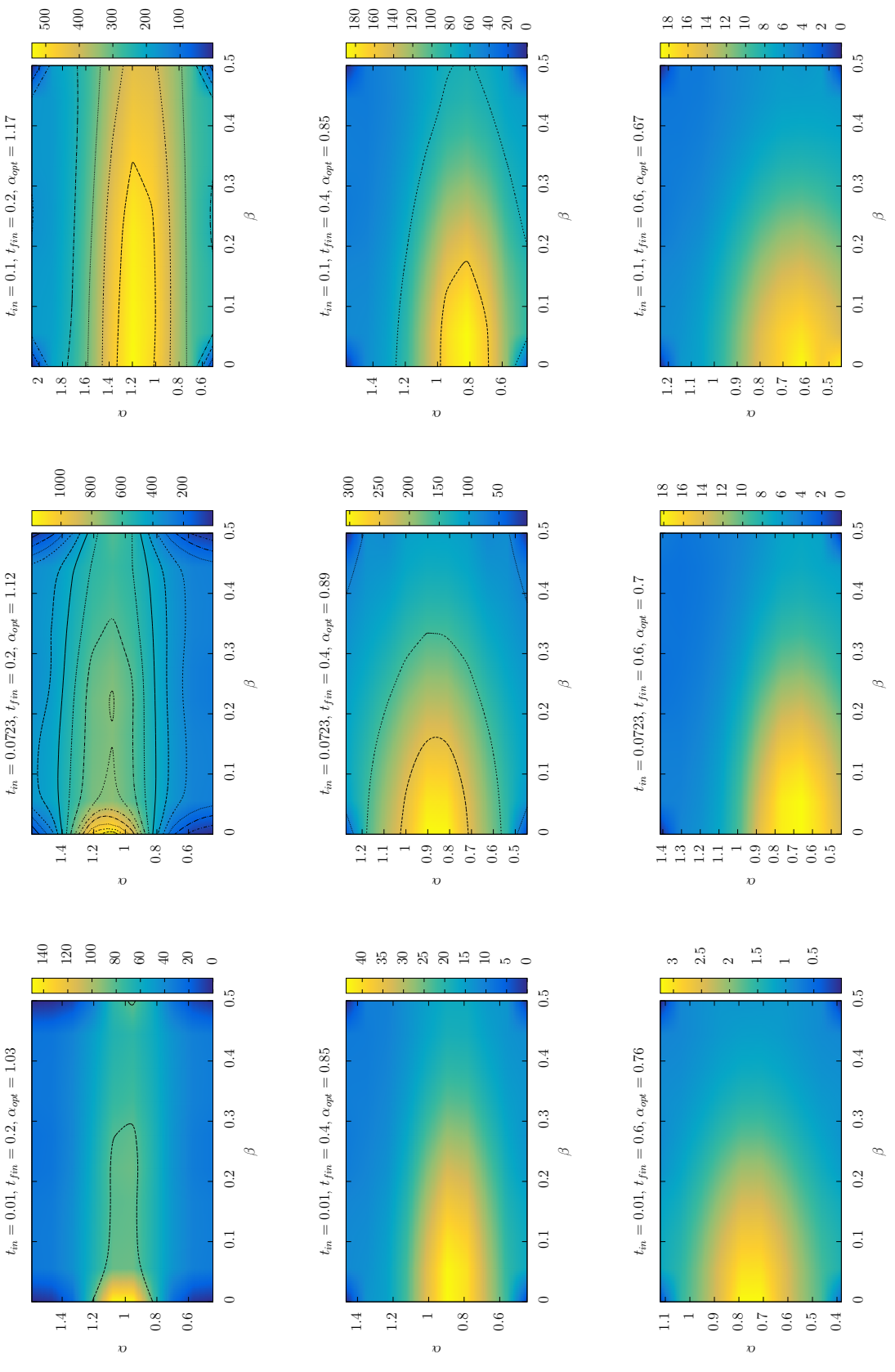

Fig. 6.6: Maximal normalized energy $\frac{E(T)}{E(0)}$ in the α-β plane with variation of initial t_{in} and final time t_{fin} and $m = 5$, $S = 0.1$ $Re_B = 1000$, $dt = 0.5$, $y_{max} = 15$, $n_{y1} = 200$, $Fr = 20$, $\gamma = 1$, $\omega = 0.008$

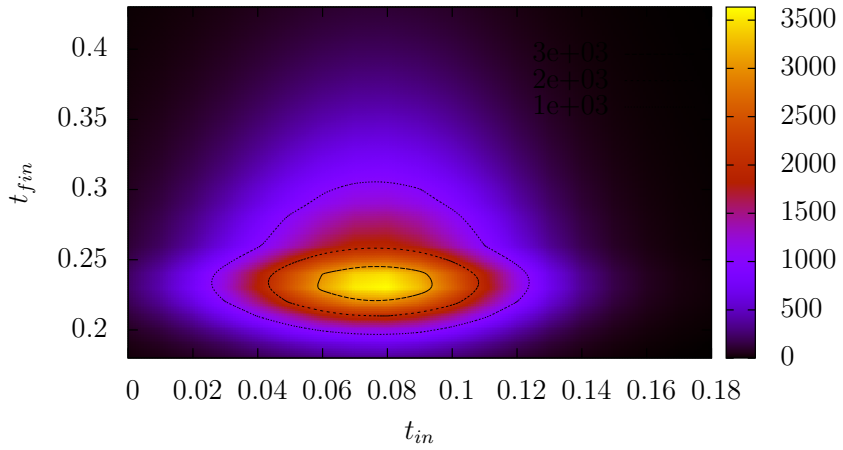

Fig. 6.7: Maximal normalized energy $\frac{E(T)}{E(0)}$ in the t_{in}-t_{fin} plane with $\alpha_B = 0.87$, $\beta = 0$, $m = 5$, $S = 0.1$ $Re_B = 1000$, $dt = 0.5$, $y_{max} = 15$, $n_{y1} = 200$, $Fr = 20$, $\gamma = 1$, $\omega = 0.008$

In comparison to the single-fluid case the final time is much smaller. This leads to the assumption, that the interface and the viscosity difference accelerate the evolution of the perturbations. As the base flow governs the perturbation equations of motion, it is of interest to take a look at it at initial and final time. In Figure 6.8 the profiles for the different initial times (left) and final times (right) of the nine cases from Figure 6.6 can be seen. Figure 6.9 shows the base flow profiles for the initial and final time in the case of Biau (2016) on the left and on the right the optimal case from Figure 6.5.

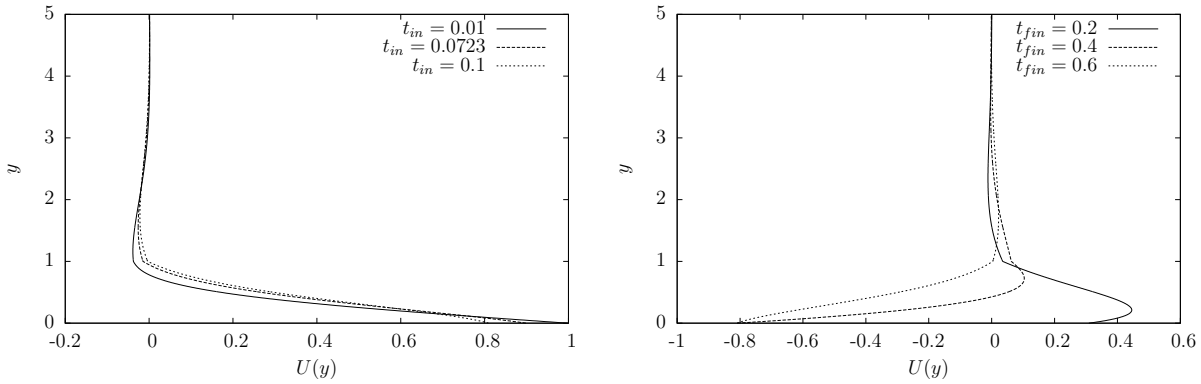

Fig. 6.8: Base flow profiles $U(y)$ for different initial times t_{in} (left) and final times t_{fin} (right) and $m = 5$, $S = 0.1$ $Re_B = 1000$, $dt = 0.5$, $y_{max} = 15$, $n_{y1} = 200$, $Fr = 20$, $\gamma = 1$, $\omega = 0.008$

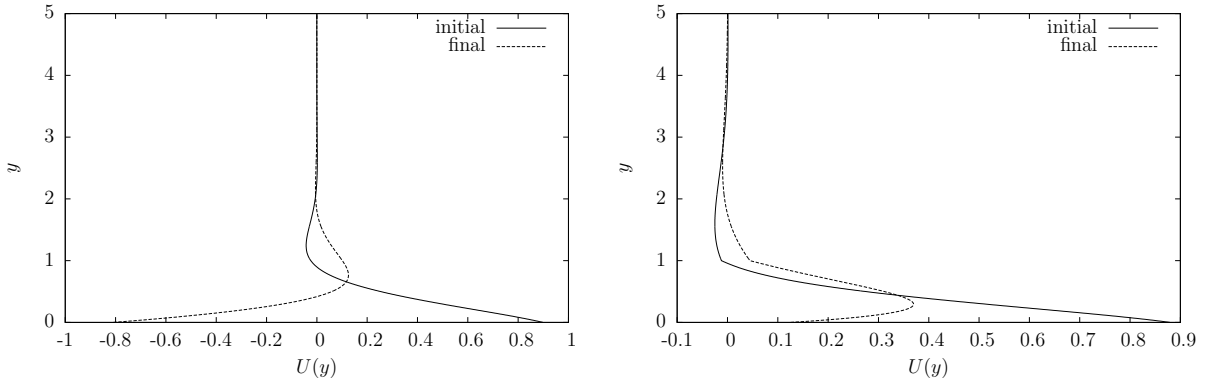

Fig. 6.9: Base flow profiles $U(y)$ in the single-fluid case with the optimal values $t_{in} = 0.0723$ and $t_{fin} = 0.4$ by Biau (2016) (left) and the optimal values in the two-fluid case $t_{in} = 0.079$ and $t_{fin} = 0.23$ (right) and $m = 5$, $S = 0.1$ $Re_B = 1000$, $dt = 0.5$, $y_{max} = 15$, $n_{y1} = 200$, $Fr = 20$, $\gamma = 1$, $\omega = 0.008$

Furthermore Figure 6.10 pictures the behavior of the perturbations on the basis of the profile of the span wise vorticity ν and velocity v at initial and final time in the optimal case in terms of α, β, t_{in} and t_{fin}. Compared to the magnitude of the cases shown in Figure 6.3 and Figure 6.4 the maximal velocity is about twice as big. The initial condition on the left is slightly different to the other cases. Again the interface at $y = 1$ is present due to the flatten virtuosity ν. The shape of v is slightly stretched in the x-direction.

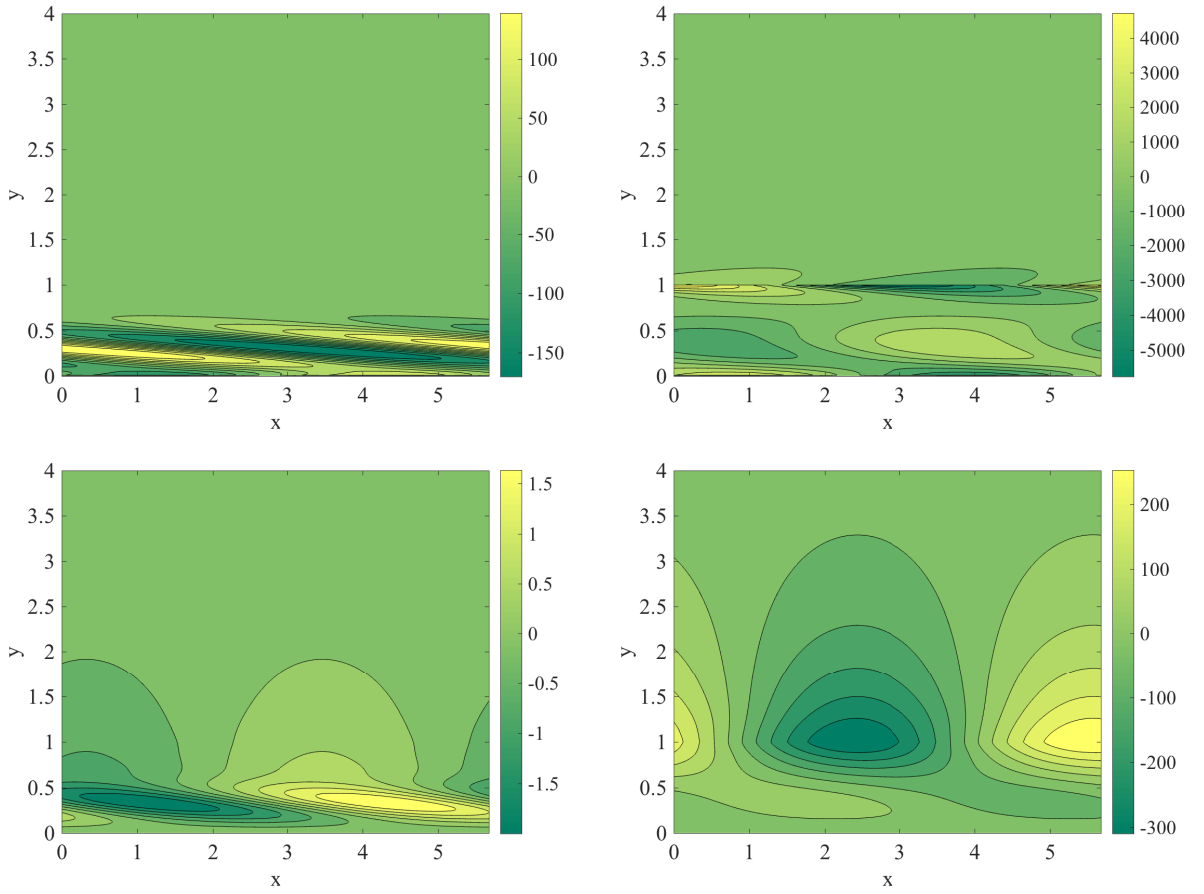

Fig. 6.10: Contours of the span wise vorticity $\nu = \frac{\partial v}{\partial x} - \frac{\partial u}{\partial y}$ (top) and v (bottom) of the perturbations at $t_{in} = 0.079$ (left) and $t_{fin} = 0.23$ (right), normalized with respect to $|v(t = 0)|$; $m = 5$, $S = 0.1$, $\alpha_B = 0.87$, $\beta = 0$, $Re_B = 1000$, $dt = 0.5$, $y_{max} = 15$, $n_{y1} = 200$, $Fr = 20$, $\gamma = 1$, $\omega = 0.008$

6.2 Physical Case: The Vitrecomized Eye

In this section the values for the variables have been changed such that the case investigated here is comparable with the human eye after vitrectomy. The choice of the Reynolds number is $Re = 7$ and the frequency of the eye movement $\omega = 0.001$ is according to Isakova et al. (2014). The surface tension is in reality much higher, but due to problems in convergence it is set to $S = 0.1$. Higher surface tension only increases the damping behavior and does not lead to more transient growth therefore this choice does not underestimate an optimal case found here. The domain is much larger with $y_{max} = 600$ as the base flow velocity stretches far out in the free stream. The numerical parameters are $dt = 1$ and $n_{y1} = 5$. The other values are $m = 5$, $\gamma = 1$, $Fr = 20$.

In order to find optimal values for α and β for the time interval $t_{in} = [0.05, 0.22]$ and $t_{fin} = [0.25, 0.35]$ nine cases where investigated with varying times. All show the same picture as in Figure 6.11 on the left. The optimal values for β is zero and for α it is even smaller than 0.02. Lowering this value even more than done here would end up in having perturbations which are no longer waves but only constant values. The right hand side of Figure 6.11 shows results with $\beta = 0$ and $\alpha = 0.02$ in the t_{in}-t_{fin}-plane and a maximum at $t_{in} = 0.145$ and $t_{fin} = 0.3$.

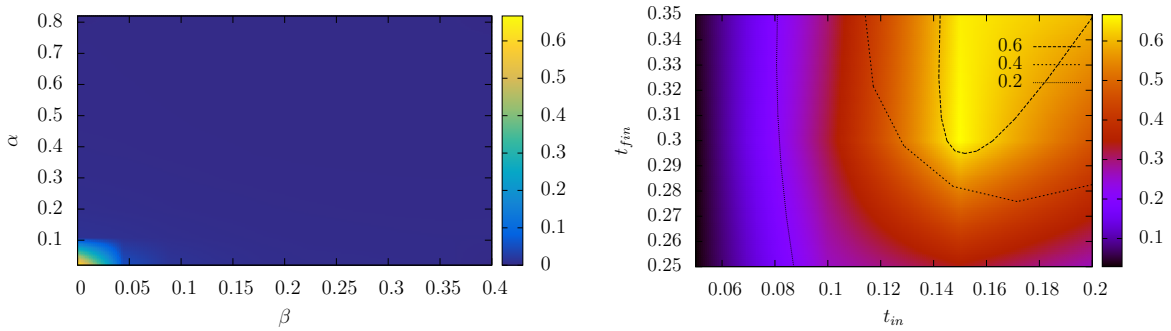

Fig. 6.11: Maximal normalized energy $\frac{E(T)}{E(0)}$ as surface parametrized with α and β and $t_{in} = 0.15$, $t_{fin} = 0.3$ (left) and in the t_{in}-t_{fin}-plane with $\alpha = 0.02$, $\beta = 0$ (right); $m = 5$, $Re = 7$, $dt = 1$, $y_{max} = 600$, $n_{y1} = 5$, $Fr = 20$, $\gamma = 1$, $\omega = 0.001$, $S = 0.1$

To understand this behavior, it is useful to have a look at the energy curve over time for this particular case shown in Figure 6.12. From this it can be seen that the case is fully damped and there is no transient growth at all.

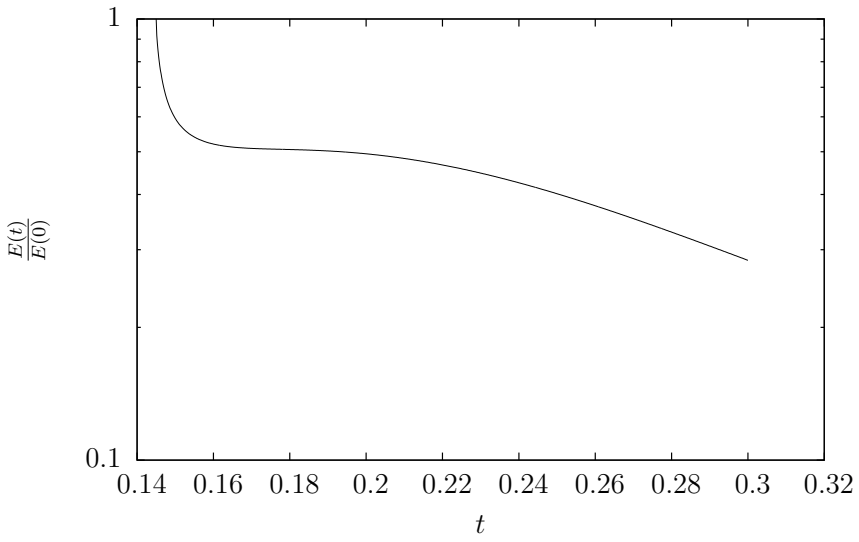

Fig. 6.12: Normalized energy $\frac{E(t)}{E(0)}$ over time t with $\alpha = 0.02$, $\beta = 0$, $t_{in} = 0.145$, $t_{fin} = 0.3$, $m = 5$, $S = 0.1$ $Re = 7$, $dt = 1$, $y_{max} = 600$, $n_{y1} = 5$, $Fr = 20$, $\gamma = 1$, $\omega = 0.001$

Chapter 7

Conclusion and Recommendations

In order to investigate the impact of transient nonmodal growth on the stability of the interface between two superposed fluids over an oscillating flat plate, the case in which the maximum energy occurs were searched for. This model problem arose from a simple approximation of the situation present in a vitrectomized eye where aqueous humor and a tamponade fluid coexist in the space once occupied by the vitreous body. The mathematical description of the problem ended up in well known equations.

Finding the worst case scenario coincided with the solution of the optimization problem in which a measure of the flow energy was minimized subject to the equations of motion of the flow.
To verify the code which was used for the numerical results, a comparison with a similar work on an oscillating Stokes flow was done successfully. The discretization approach here was *"first discretize, then optimize"* and led to satisfactory results. However in the two-fluid case the choice of the approach became crucial again as it led to numerical problems most likely due to the discretization on the interface. The alternative approach *"first optimize, then discretize"* made it necessary to set up the continuous adjoint equations of motion as well as the continuous interface and boundary conditions.

The results presented here recommend the exclusion of short-term effects on emulsification in the human eye. In section 6.2 it is shown that a flow with these characteristics is completely damped and does not give rise to transient growth. Further research on reasons of emulsification should be conducted in the long term behavior or completely different mechanisms such as the rapid process of inserting the silicon oil into the eye or geometrical characteristics that favor emulsification. The linear modal stability analysis from Isakova et al. (2014) should be carried further with a non-linear stability analysis. There are several possible extensions of the model such as the curvature but also specific geometrical characteristics as roughness of the inner surface of the eye.

On nonmodal stability analysis of two superposed fluids over an oscillating plate nothing has been published at the present time and such it is new for the field of fluid mechanics. In the case of relevant parameters as presented in section 6.1 it is shown that waves of the shape $u(y,t)e^{i\alpha x}$ lead to the maximum amplification as the optimal value of β is zero. With growing viscosity ratio m the optimal values for α does not change much. On contrary the influence of t_{in} and t_{fin} is evident. In comparison to the single fluid case in Biau (2016) the optimal t_{fin} is smaller as well as the nonmodal growth. What is left

to investigate is the behavior of flows with different Reynolds numbers. It can not be excluded that this might show qualitatively different results. Also a density difference of the two fluids $\gamma \neq 1$ has not been investigated in the parameter study.

The contribution of this work is not only to the field of ophthalmology but also to fluid mechanics in general. One reason for emulsification in the human eye could be excluded which narrows the remaining possibilities. In addition a starting point for the investigation of a two-fluid Stokes flow is set.

Bibliography

[Batchelor 2000] Batchelor, G. K.: *An Introduction to Fluid Dynamics:*. Cambridge : Cambridge University Press, 2000. – ISBN 9780511800955 (Quoted on page 11 and 13.)

[Biau 2016] Biau, D.: Transient growth of perturbations in Stokes oscillatory flows. In: *Journal of Fluid Mechanics* 794 (2016), 005 (Quoted on page iii, iv, v, 2, 3, 30, 32, 35, 36, 38, 40, 46, 47, and 51.)

[Heimann et al. 2008] Heimann, H. ; Stappler, T. ; Wong, D.: Heavy tamponade 1: a review of indications, use, and complications. In: *Eye* 22 (2008), März, Nr. 10, S. 1342–1359. – ISSN 0950–222X (Quoted on page 2.)

[Hinze et al. 2008] Hinze, M. ; Pinnau, R. ; Ulbrich, M. ; Ulbrich, S.: *Optimization with PDE Constraints*. Springer Netherlands, 2008 (Mathematical Modelling: Theory and Applications). – ISBN 9781402088391 (Quoted on page 22.)

[Isakova et al. 2014] Isakova, K. ; Pralits, J. O. ; Repetto, R. ; Romano, M. R.: A model for the linear stability of the interface between aqueous humor and vitreous substitutes after vitreoretinal surgery. In: *Physics of Fluids* 26 (2014), Nr. 12 (Quoted on page 2, 49, and 51.)

[Joseph and Renardy 1993] Joseph, D. D. ; Renardy, Y. Y.: *Fundamentals of Two-Fluid Dynamics*. Bd. 3. Springer New York, 1993 (Quoted on page 2, 16, and 18.)

[Kleinberg et al. 2011] Kleinberg, T. T. ; Tzekov, R. T. ; Stein, L. ; Ravi, N. ; Kaushal, S.: Vitreous Substitutes: A Comprehensive Review. In: *Survey of Ophthalmology* 56 (2011), Nr. 4, S. 300 – 323. – ISSN 0039–6257 (Quoted on page 2.)

[Orazzo et al. 2014] Orazzo, A. ; Coppola, G. ; Luca, L. de: Disturbance energy growth in core-annular flow. In: *Journal of Fluid Mechanics* 747 (2014), 005, S. 44–72 (Quoted on page 2 and 21.)

[Schmid 2007] Schmid, P.J.: Nonmodal stability theory. In: *ANNUAL REVIEW OF FLUID MECHANICS* 39 (2007), S. 129–162. – ISBN 978–0–8243–0739–4 (Quoted on page 2, 4, and 8.)

[Schmid and Henningson 2000] Schmid, P.J. ; Henningson, D.S.: *Stability and Transition in Shear Flows*. Springer New York, 2000 (Applied Mathematical Sciences). – ISBN 9780387989853 (Quoted on page 14, 15, and 16.)

[Yarin 2012] Yarin, L.P.: *The Pi-Theorem*. Bd. 1. Springer-Verlag Berlin Heidelberg, 2012 (Quoted on page 11.)

Appendix A

Excerpts from the Code

The extracts of the code here presented are the main program in Listing A.1 and the subroutine of the optimization loop Listing A.2. The language used is called `cpl` "a high-level programming language designed and developed by Paolo Luchini between 1993-2006" (Quote from the `cpl`-documentation file). All files necessary for reproducing the results from chapter 6 can be found on the CD at the back of this thesis. As the compiler belongs to the inventor, it is not provided here.

Listing A.1: main.cpl

```
! Jan Pralits V1.0 2016-09-06
! changes: Aulikki Wilhelmi April/Mai 2017
!
USE rbmat
USE cbmat
USE lapack
!-------------read from file occhio.in ----------
! Re        : Reynolds number
! ReB       : Reynolds number Biau scaling
! nin       : Fraction of period tin=nin*period
! dt        : time step
! np        : Fraction of period tfin=np*period
! omega     : frequency of wall oscillation
! ny1       : Number of discrete points up to the interface
! ymax      : Maximum value for wall normal direction
! alfa      : streamwise wave number
! alfaB     : streamwise wave number Biau scaling
! beta      : spanwise wave number
! err       : rel. error of gain G in iteration of opt. pert.
! tol       : tolerance
! mv        : ratio mu2/mu1
! Fr        : Froude number
! gamma     : ratio rho2/rho1
! S         : surface tension
! c_se      : coefficent for interface energy
```

```
REAL Re, ReB, tin, tfin, dt, nin, np, omega, dny1, ymax, alfaB,
    alfa, beta, err, tol, mv, Fr, gamma, S, c_se, k2
INTEGER ny, ny1
FILE INPUT=OPEN("occhio.in")
DO WHILE READ BY NAME FROM INPUT ReB OR nin OR dt OR np OR omega
     OR ny1 OR ymax OR alfaB OR beta OR err OR tol OR mv OR Fr OR
     gamma OR S
CLOSE(INPUT)

Re=ReB^2*omega/(2*PI)
alfa=alfaB*((omega*Re)/(2*PI))^0.5
k2=alfa*alfa+beta*beta
c_se=0.5*S*k2/Re^2
tin=nin*2*PI/omega
tfin=np*2*PI/omega
dny1=1/ny1
ny=ROUND(ymax/dny1)

!------- define dimensionless wall normal coordinate ---------
REAL y(0..ny)=0
DO y(i)=ymax*i/ny FOR ALL i

!-------- define distribution in time --------
REAL t
INTEGER nt
nt=ROUND(1+(tfin-tin)/dt)

! parabolic distribution
REAL FUNCTION tt(INTEGER it)=tin+(it-1)*dt

!------- define variables for subroutines ---------
! neq       : number of equations
! nstate    : number of state variables
! bwidth    : band width of matrix
! U1at1_..  : first deriv. of U at the surface (y=1)
! U2at1_..  : second deriv. of U at the surface (y=1)
! U,U1,U2   : streamwise meanflow velocities, first deriv.,
   second deriv.
! A,B,T     : matrices T = B*sigma + A, sigma is the eigevalue
! M             : matrix for the energy
!
INTEGER neq = 2
INTEGER nstate = 2
INTEGER bwidth = 18
REAL U1at1_1=0,U1at1_2=0,U2at1_1=0,U2at1_2=0
```

```
ARRAY(0..ny) OF REAL U=0,U1=0,U2=0
ARRAY(1..neq*(ny+1)+3,-bwidth..bwidth) OF COMPLEX A=0, B=0, C=0,
    D=0, M=0
ARRAY(1..neq*(ny+1)+3,-bwidth..bwidth) OF COMPLEX Aadj=0, Badj
   =0, Cadj=0, Dadj=0
ARRAY(1..neq*(ny+1)+3) OF COMPLEX Q=0,P=0
!-----------------------------------------
! Energy norm
REAL FUNCTION Energy(COMPLEX QQ(*), MMM(*,*)) = REAL(CONJG(QQ)*
   MMM*QQ)
! coefficients for second order finite differences
USE Deriv4th
! subroutines to set up matrices of the direct equations
USE BuildMats
! subroutines to set up matrices of the adjoint equations
USE BuildMatsAdjoint
! subroutines to calculate the base flow
USE BaseFlow
! subroutine to find the optimal solution
USE OptPert
! compute coefficients of derivatives
SetDerivatives
!-----------------------------------------
! MAIN program ---------------------------
!-----------------------------------------
! initial condition for Q
LOOP FOR i=0 TO ny1
Q(neq*i+1) = y(i)*exp(-y(i))
Q(neq*i+2) =0*y(i)*exp(-y(i))
REPEAT LOOP

Q(2*ny1+3) = 0*y(ny1)*exp(-y(ny1))

LOOP FOR i=ny1 TO ny
Q(neq*i+4) = y(i)*exp(-y(i))
Q(neq*i+5) =0*y(i)*exp(-y(i))
REPEAT LOOP

Q = Q/MAXABS(Q)
!---------------------------------------
OptPert()
!-----------------------------------------
! end MAIN program -----------------------
!-----------------------------------------
```

Listing A.2: OptPert.cpl

```
SUBROUTINE OptPert

REAL E0=0, ET=0, G=1,Gold=10*G,dG
ARRAY(1..neq*(ny+1)+3,-bwidth..bwidth,1..nt) OF COMPLEX CS=0,
    CSA=0
ARRAY(1..neq*(ny+1)+3,-bwidth..bwidth) OF COMPLEX Ineg=0
ARRAY(1..neq*(ny+1)+3) OF COMPLEX d=0,Qin=0,Q1=0,Q2=0,QN=0,Pin
    =0,Pm1=0,P1=0,P2=0,PN=0
INTEGER ip=1,i,j,it

LOOP FOR k=0 TO ny1
Ineg(2*k+1,0)=-1
Ineg(2*k+2,0)=1
REPEAT LOOP

Ineg(2*ny1+3,0)=1

LOOP FOR k=ny1 TO ny
Ineg(2*k+4,0)=-1
Ineg(2*k+5,0)=1
REPEAT LOOP

!---------- main loop of optimization----------
DO

    IF ip=1 THEN
        Q=Qin
    ELSE IF ip>1 THEN
!----update of the initial condition of the direct loop ----
        Q=Ineg*CONJG(Pin)*ET/2
        Qin=Q
    END IF

    Qnorm=MAXABS(Q)
    t = tin
    Q1=Q
    Q2=Q

    IF ip=1 THEN
        BuildM(M)
        D=0;BuildD(D)
    END IF
```

```
!————————— direct loop ————————————

   LOOP FOR it = 2 TO nt
        t = tt(it)
          IF ip=1 THEN
             BaseFlow(t,Re,omega)
             BuildC(C)
             LUdecomp C
             CS(*,*,it)=C
          ELSE IF ip>1 THEN
             C=CS(*,*,it)
          END IF
        Q2=Q1
        Q1=Q
        d = D*(2*Q1 - 0.5*Q2)/dt     ! Adams-Bashfordt time dis.
        Q=C\d
   REPEAT LOOP

   QN=Q
   Gold=G
   G=Energy(QN,M)/Energy(Qin,M)
   ET = Energy(QN,M)
   E0 = Energy(Qin,M)

!———update of the initial condition of the adjoint loop ——
   PN=-2*E0/(ET^2)*Ineg*CONJG(QN)

   P=PN
   P1=P
   P2=P

   IF ip=1 THEN
      Dadj=0;BuildDadj(Dadj)
   END IF

!————————— adjoint loop ————————————

   LOOP FOR it = nt-1 DOWN TO 1
        t = tt(it)
        IF ip=1 THEN
           BaseFlow(t,Re,omega)
           BuildCadj(Cadj)
           LUdecomp Cadj
           CSA(*,*,it)=Cadj
        ELSE IF ip>1 THEN
```

```
            Cadj=CSA(*,*,it)
        END IF
        P2=P1
        P1=P
        d = Dadj*(2*P1 - 0.5*P2)/dt   ! Adams-Bashfordt time dis.
        P=Cadj\d
    REPEAT LOOP

    Pin = P
    err = ABS((G-Gold)/G)
    ip = ip+1

WHILE err>tol

!-------------optimization loop end-------------

END OptPert
```